C.P. No. 639

C.P. No. 639

MINISTRY OF AVIATION

AERONAUTICAL RESEARCH COUNCIL

CURRENT PAPERS

Measurements in Flight of the Longitudinal Stability Derivatives of a 60° Delta Wing Aircraft (Fairey Delta 2)

by

D. R. Andrews

U.D.C. No. 533.6.013.412 : 533.6.013.417 : 533.6.053 Fairey Delta 2

C.P. No. 639

April, 1959

MEASUREMENTS IN FLIGHT OF THE LONGITUDINAL STABILITY DERIVATIVES OF A 60° DELTA WING AIRCRAFT (FAIREY DELTA 2)

by

D.R. Andrews

SUMMARY

Longitudinal short period oscillations have been excited in flight on the Fairey Delta 2 aircraft by stick pulses, and the results analysed to give some of the longitudinal derivatives. Values of the derivatives $m_{\dot{\theta}}$, $\partial C_L/\partial \alpha$, H_m and m_w are presented for a Mach number range up to M = 1.6 at 38,000 ft altitude and M = 1.15 at 10,000 ft altitude. Some values of m_η have also been derived.

Comparison is made with wind tunnel, rocket model, and wing flow test results, and also with theoretical estimates.

Replaces R.A.E. Report No. Aero 2617 - A.R.C. 21,699

LIST OF CONTENTS

LIST OF APPENDICES

TABLE

LIST OF ILLUSTRATIONS

1 INTRODUCTION

A programme of flight tests is being carried out on the second prototype Fairey Delta 2 aircraft, aimed at obtaining the aerodynamic derivatives of the aircraft for comparison with wind tunnel and rocket model test data and also with theoretical estimates.

The first phase of the programme has been to measure the longitudinal derivatives $\partial C_L/\partial \alpha$, $m_{\dot{\theta}}$, H_m and m_w by analysing the stick fixed longitudinal short period oscillation that occurs after an elevator pulse. This report gives details of the results obtained and gives a comparison with data obtained from other sources.

2 DETAILS OF AIRCRAFT

The Fairey Delta 2 is a tailless delta-wing aircraft having 60° leading edge sweepback of the wing and vertical fin. Table 1 gives details of the aircraft, and a photograph and three view drawing are shown in Figs.1 and 2 respectively.

The elevators, aileron and rudder are power operated, artificial feel being supplied by springs and cam followers. A gear change mechanism is fitted to enable the pilot to vary the gearing between the stick and the controls. Operation of the gearchange mechanism alters both the elevator and aileron gearing at the same time. Trim is obtained by varying the datum of the spring feel.

The aircraft was flown at an all-up-weight at take-off of 13,840 lb and a C.G. position with undercarriage down of 165.9 in. aft of the leading edge of the centreline chord. For the flight patterns flown in the present series of tests, the C.G. positions at which the test results were obtained were within ±0.4 in. of 163.3 in. aft of the leading edge of the centreline chord. The estimated moment of inertia in pitch under these conditions gave a value of i_B of 0.205. The estimated variation of C.G. position with fuel contents during a typical flight is shown in Fig.3.

3 INSTRUMENTATION

Airspeed, altitude and fuel contents were read from auto-observer instruments photographed by an Eclair camera running at 8 frames per second. The ASI and altimeter were fed with pressures from an airspeed head mounted on the nose boom.

Hussenot A22 recorders were fitted and were set to run at a paper speed of about 1 in./sec. The following is a list of the relevant quantities measured together with the type and range of the transmitting instrument:-

Normal acceleration	SFIM accelerometer	0 - 2g
Rate of pitch	Ferranti gyro	±15°/sec
Rate of roll	Ferranti gyro	±30°/sec
Rate of yaw	Ferranti gyro	±15°/sec
Angle of sideslip	Wind vane	± 5°
Angle of attack	Wind vane	-5° + 25°
Elevator angle port	Potentiometer	-6° + 4°

Synchronisation between the Hussenot recorders and the auto-observer was effected by a $\frac{1}{2}$ second timing clock supplying a veeder in the auto-observer and event markers in the recorders.

Dynamic calibrations of the gyros and accelerometer were made on an oscillatory table. The following results were obtained:-

	Natural frequency (undamped)	Input frequency c.p.s.	Phase lag (degrees)
0 - 2g accelerometer	20 c.p.s.	1.0 1.5 2.0	1° $2\frac{1}{2}^{\circ}$ $4\frac{1}{2}^{\circ}$
Rate of pitch gyro $\pm 15^{\circ}$ range	12 c.p.s.	1.0 1.5 2.0	9° 12° 15°

The accelerometer was air damped but was sealed in an airtight box to eliminate any effects of changing altitude. The gyro was damped with silicone oil. Measurements made in flight showed that at all times the gyro temperature was approximately 15°C, so that the effect of variations in the viscosity of the silicone oil could be neglected.

4 PRESSURE ERROR AND LAG CORRECTIONS

The airspeed head was mounted on the nose boom of the aircraft and consisted of a Mk.9A pitot-static head with its drain hole sealed (now called a Mk.9E head).

The installation was calibrated in low level runs past the airfield Control Tower, measurements of the altitude indicated in the aircraft being made with a sensitive aneroid covering the range -1000 to +2000 ft altitude. The results are shown in Fig.4, expressed in coefficient form. Data from wind tunnel tests on the airspeed head alone[1] have been used to extrapolate the results to low speed and to give the total head error.

Fig.5 shows the static pressure error of the first prototype aircraft (WG.774) obtained at 38,000 ft altitude in fly-bys past the A & AEE calibrated Venom. Also shown are the results of Fig.4 extrapolated to 38,000 ft by assuming that C_p is a function only of C_L. The lack of agreement between the two sets of results is apparent and cannot be satisfactorily explained. As the difference between the sea level and the 38,000 ft results amounts to only about 0.013 in Mach number at M = 0.9, it was considered sufficiently accurate to assume that the difference was a linear effect of altitude and was not dependent on Mach number. Hence at any given Mach number, the C_p has been assumed to be that for WG.774 at 38,000 ft (Fig.5) plus an increment in C_p of (38,000 - altitude) × 0.025/38,000.

The pressure lags in the pitot and static system were determined from ground tests in the usual manner, and corrections applied to the flight test data wherever applicable.

True airspeed was determined using values for the ambient air temperature supplied by the Meteorological Office.

5 FLIGHT TEST TECHNIQUE

The technique used was for the pilot to trim the aircraft at the required Mach number, and then sharply strike the control stick so as to apply a normal acceleration of about 2g total, the stick being returned to its trimmed position by the artificial feel springs. The ensuing longitudinal oscillation was allowed to subside without the pilot again touching the stick.

In practice, accurate longitudinal trimming prior to initiating the oscillation was found to be virtually impossible at transonic and supersonic speeds. At transonic speeds the nose down trim change made the aircraft statically unstable, and at supersonic speeds the speed was either increasing reheat on or decreasing reheat off, since the two position nozzle allowed no control over the reheat thrust.

Difficulty in trimming the aircraft laterally often led to some divergence in roll during the longitudinal oscillation.

Tests were made in level flight at Mach numbers up to 1.65 at 38,000 ft and 1.15 at 20,000 ft, 15,000 ft and 10,000 ft altitude.

6 ANALYSIS TECHNIQUE AND ACCURACY OF RESULTS

6.1 Analysis technique

In view of the known large effect of elevator motion, only that part of each oscillation where the elevator had stopped moving was analysed. This does not, of course, preclude the possibility of small elevator motions within the resolution of the instrumentation being present, and Appendix 2 discusses the possible errors that might arise from this. The lateral motion that was generally present was assumed to have no effect on the longitudinal motion.

Each oscillation was analysed graphically by plotting on semi-log paper the envelopes of the positive and negative peaks of both the normal acceleration and rate of pitch. The best straight lines were then drawn to define the mean envelope of each oscillation, the mean of the slopes giving the damping factor $\mathcal{R}$. The indicated amplitude ratio $(q^*/n^*)'$ was also derived from these mean envelopes. The indicated phase angle ϕ'_{qn} by which q leads n, and the periodic time P were obtained by drawing the mean line of the oscillation and plotting the intercepts of the q and n traces.

Corrections to ϕ'_{qn} and $(q^*/n^*)'$ were then made to allow for the different response characteristics of the accelerometer and gyro and for the accelerometer being situated ahead of the C.G. (Appendix 1). The true value of ϕ_{qn} is

$$\phi_{qn} = \phi'_{qn} + \chi \qquad (1)$$

where χ = amount by which phase lag of gyro exceeds that of accelerometer (degrees).

The value of χ depends on the frequency of the oscillation (para.3).

The true value of q^*/n^* is

$$\frac{q^*}{n^*} = \left(\frac{q^*}{n^*}\right)_{indic} \Big/ \left(1 + \frac{2\pi}{P}\left(\frac{q^*}{n^*}\right)_{indic} \frac{\ell}{g}\right) \qquad (2)$$

where $\left(\frac{q^*}{n^*}\right)_{indic} = \left(\frac{q^*}{n^*}\right)' e^{-\mathcal{R}\frac{\chi}{360}P}$

and ℓ = distance of normal accelerometer ahead of C.G. (feet).

Using the values of q^*/n^*, P, and $\mathcal{R}$ so derived, the aerodynamic derivatives a, $m_{\dot{\vartheta}}$, and H_m, were obtained using the equations given in Ref.2. The lift curve slope, a, is given by

$$a = \frac{2}{p^2 - 1}\left[\sqrt{p^2 R^2 + (p^2-1) J^2} - R\right] \qquad (3)$$

where $p = \frac{V}{g}\frac{q^*}{n^*}$

$R = \mathcal{R}\hat{t}$

$J = \mathcal{I}\hat{t} = \frac{2\pi}{P}\hat{t}$.

The rotary damping derivative $m_{\dot{\vartheta}}$ is calculated from the equation

$$m_{\dot{\vartheta}} = m_q + m_{\dot{w}} = -i_B\left(2R - \tfrac{1}{2}a\right) \qquad (4)$$

and the manoeuvre margin from

$$H_m = \frac{i_B}{\mu}\frac{2}{a}(R^2 + J^2). \qquad (5)$$

If m_q can be estimated or derived from other sources, m_w can be obtained since

$$m_w = -\frac{a}{2}K_m$$

$$= -\frac{a}{2}\left[H_m + \frac{m_q}{\mu}\right]. \qquad (6)$$

As m_q/μ is small compared with H_m, large errors in the estimated values of m_q can be tolerated.

It can easily be shown that equations (3), (5) and (6) reduce to the following very approximate relations

$$a = \frac{2J}{p} \tag{7}$$

$$H_m = \frac{i_B}{\mu} p J \tag{8}$$

$$m_w = -\frac{i_B}{\mu} J^2. \tag{9}$$

These are useful in assessing the effect of errors in the various measured quantities.

The pitching moment derivative due to elevator deflection (m_η) is obtained from the relation

$$H_m = -\frac{2m_\eta}{C_L}\frac{\Delta\eta}{n}$$

$$= -2m_\eta \frac{\Delta\eta}{\Delta C_L}. \tag{10}$$

The quantity $\Delta\eta/\Delta C_L$ is obtained from measurements of η and n in turns and pull-ups.

6.2 Accuracy of results

The maximum errors that are probably present in the values of J, p, R and ϕ_{qn} obtained from the flight tests at 38,000 ft are shown in the following table, together with the consequent errors in the derivatives:

	$\frac{\Delta J}{J} = \pm 2\%$	$\frac{\Delta p}{p} = \pm 3\%$	$\frac{\Delta R}{R} = \pm 5\%$	$\Delta\phi_{qn} = \pm 5^\circ$
% error in a	±2%	∓5%	0	±2%
% error in H_m and m_η	±2%	±5%	0	∓2%
% error in m_w	±4%	0	0	0
Error in $-m_\vartheta$	∓0.01	±0.01 to 0.02	±0.02 to 0.03	∓0.01

It may be noted that although ϕ_{qn} is not used directly in the analysis, an error in ϕ_{qn} caused by, say, instrumentation phase lag errors, affects the

±0.03. At low altitudes where the damping is high and relatively few cycles are available for analysis, the errors may be considerably larger than these.

As the errors in m_η will depend upon the accuracy of both H_m and $\Delta\eta/\Delta C_L$, it is probable that the overall accuracy in this derivative will not be better than about ±15%.

In obtaining the derivatives, it has been necessary to use an estimated value of i_B, pending measurements on the full scale aircraft. Experience has shown that estimates of moment of inertia can be considerably in error and that a discrepancy of 10% between the estimated and true values would not be unusual. As the derivatives m_ϑ, H_m, m_w and m_η are proportional to i_B, a discrepancy of this magnitude is clearly important. The value of $\partial C_L/\partial\alpha$ is, however, unaffected by i_B.

Additional errors may arise from

(1) elevator oscillations small enough to be undetected by the instrumentation,

(2) coupling of the lateral and longitudinal motions.

The first of these is discussed fully in Appendix 2, where it is shown that, although the errors are small at 40,000 ft altitude, significant errors can result at 10,000 ft altitude. The effects of coupling between the lateral and longitudinal oscillations are generally small and are discussed in para.8 and Appendix 3.

7 RESULTS

Fig.6 shows four typical time histories showing the decay of the longitudinal short period oscillation following a stick pulse. The following features will be apparent from a study of these time histories

(1) the very high damping at low altitudes and low speeds results in a correspondingly small number of cycles to damp (Fig.6(a)). In many such cases, it becomes impossible to apply the technique of para.6, although the period can often be derived with fair accuracy

(2) except at the lowest speeds, some elevator motion takes place after the stick has returned to its trimmed position. This motion is usually of an oscillatory nature. Because of the known large effects of such elevator motions (Appendix 2), only that part of each trace where the elevator appears steady has been analysed. This still does not rule out the possibility of elevator oscillations being present within the resolution limits of the instrumentation measuring elevator position, and this aspect is discussed in some detail in Appendix 2. The reason for this elevator motion is not completely understood, although it is undoubtedly related to the characteristics of the hydraulic system of this aircraft

(3) a lateral oscillation commences soon after the start of the longitudinal oscillations. This could arise from

(a) an inadvertent aileron pulse applied at the same time as the elevator pulse

(b) differential movement of each elevator during and after the pulse

(c) engine gyroscopic effects.

The known characteristics of the hydraulic system make it probable that differential elevator movement is primarily responsible for this lateral motion, although, because of the very coarse range of the transducer on the starboard elevator, this could not be substantiated. In the majority of cases no aileron movement could be detected. The effects of engine gyroscopic coupling can be shown to be very small (Appendix 3).

Analysis of the longitudinal oscillations has been made on the assumption that their characteristics are unaffected by the lateral motion. The validity of this assumption is discussed in para.8.

Figs.7, 8, 9 and 10 show the period, damping, phase angle between rate of pitch q and normal acceleration n, and the amplitude ratio of q to n. These are the quantities required for the determination of the aerodynamic derivatives and are fully corrected for instrument errors. At 38,000 ft it will be seen that the period reduces from 2.0 seconds at M = 0.8 to just less than 1.0 at supersonic speeds. As altitude is reduced so the period also decreases. A sharp change in the period will be noticed at M= 0.94 at 38,000 ft and M = 0.97 at 10,000 ft altitude. The total damping is always positive although a trough exists near M = 0.95 (Fig.8). The damping increases markedly with reduction in altitude.

Figs.11, 12, 13 and 14 show the values of $m_{\dot{\theta}}$, $\partial C_L/\partial\alpha$, H_m and m_w as derived from equations (3), (4), (5) and (6) of para.6.

The lift curve slope for constant elevator position increases up to a Mach number of 1.0 and then decreases progressively (Fig.11). Reduction in altitude from 38,000 ft to 10,000 ft causes an apparent loss in $\partial C_L/\partial\alpha$ of about 20%.

The rotary damping derivative $m_{\dot{\theta}}$ increases to a peak value of -0.5 at M = 0.93 and this decreases abruptly to become destabilising over a small band of Mach number from 0.95 to 0.965 (Fig.12). Note, however, that in this region the total damping is still positive (Fig.8). At supersonic speeds, $m_{\dot{\theta}}$ varies between -0.1 and -0.2 and is little affected by altitude. The points obtained at low altitude at subsonic speeds are unreliable due to the difficulty of measuring $\mathcal{R}$ and q^*/n^* when the damping is high.

The stick fixed manoeuvre margin, H_m, increases from 0.08 to 0.12 as M increases from 0.85 to 1.0 at 38,000 ft, and then increases gradually with increasing supersonic Mach number (Fig.13). The value of H_m decreases with decreasing altitude, suggesting that aero-elastic effects are much larger than the effect of the m_q/μ term.

Fig.14 shows the derivative m_w, calculated from equation (6) using the values of m_q estimated from Ref.6. As m_q/μ is small compared to H_m, large errors in the estimation of m_q have little effect. The value of $-m_w$ at 38,000 ft rises progressively to a maximum value of 0.22 at M = 0.96 and then decreases slowly with increasing Mach number. At 10,000 ft altitude, the magnitude of this derivative is only about 60% of its value at 38,000 ft.

The pitching moment derivative due to elevator deflection (m_η) can be obtained from equation (10) of para.6.1 if $\Delta\eta/\Delta C_L$ is known. This quantity $\Delta\eta/\Delta C_L$ was obtained from measurements of η and n in turns and pull-ups[5] and is shown in the upper part of Fig.15. The results below M = 1.0 were obtained

at all altitudes up to 50,000 ft, but those above M = 1.0 were limited to the altitude band from 30,000 - 50,000 ft. Within the limits of this test envelope there appeared to be no effect of altitude on $\Delta\eta/\Delta C_L$. The C.G. at which these results were obtained was virtually identical to that of the aircraft used in the present series of tests. The values of m_η derived from equation (10) are shown in the lower part of Fig.15. The marked fall-off in control effectiveness above M = 1.0 is very apparent.

8 DISCUSSION

The low experimental scatter of the results obtained at 38,000 ft is pleasing and is a measure of the repeatability that can be obtained from this technique when several cycles of the oscillation are available for analysis. The high damping at low altitude increases the possible experimental errors, but even so, the results show a marked consistent effect of altitude on the derivatives a, H_m and m_w. In an attempt to explain the reason for this altitude effect, some consideration will now be given to the following

(1) aero-elasticity

(2) coupling between the lateral and longitudinal oscillations

(3) small elevator oscillations within the resolution of the instrumentation measuring elevator movement.

Some calculations have been made by the Fairey Aviation Company on the effects of aero-elasticity at M = 1.3 and 1.7 at various altitudes. To give some idea of the effect at other Mach numbers, these calculated values have been extrapolated assuming that the aero-elastic effect is solely a function of $\frac{1}{2}\rho V^2$. The measured derivatives corrected in this way to rigid aircraft conditions are shown in Figs.16 and 17. It will be seen that aero-elasticity can account for much of the altitude effect on H_m and m_η, but only goes part of the way towards explaining the effect on $\partial C_L/\partial\alpha$ and hence on m_w.

Engine gyroscopic coupling can play some part in modifying the period and damping. This effect is discussed in Appendix 3 and is shown to be generally negligible. The errors are largest at low speed and high altitude and at M = 0.8 at 38,000 ft, for example, the derivatives a and H_m will be too large by about 2% and the derivative $-m_w$ too large by about 5%. This of course <u>increases</u> the measured difference in the derivatives at different altitudes.

Once the lateral motion has commenced, some forcing of the longitudinal oscillation could arise from the inertia term (C-A) pr and the aerodynamic derivative m_β. However rough calculations suggest that the maximum error in q^*/n^* due to the inertia term will always be less than 1%, and this is clearly negligible. No estimate can be made of m_β, but it is believed that its magnitude is very small.

Large errors can arise at low altitude from the presence of elevator oscillations small enough to be within the resolution of the instrumentation recording elevator movement, and therefore undetectable. Appendix 2 shows that if the elevator motion is phased in a certain manner to the normal acceleration, the errors can be large enough to explain the difference shown in Figs.16 and 17 between the 10,000 ft and 38,000 ft "rigid aircraft" derivatives $\partial C_L/\partial\alpha$, H_m and m_w. Further, the high damping at low altitude leads, not

only to inaccuracies in the measurement of $\mathcal{R}$, P and q^*/n^*, but also to the necessity for commencing the analysis at a point soon after the termination of the elevator pulse. As the elevators take a finite time to stabilise, there is the increased probability at low altitude of small elevator motions still being present in the region where the analysis is made. The use of a more sensitive elevator transducer and of harmonic analysis techniques would appear worthwhile.

In view of the above remarks, the low altitude results are not considered to give as true a representation of the stick fixed derivatives as the 38,000 ft results. These latter are therefore the results that will be used in comparing with data from other experimental sources. The flight test data used in this comparison will be uncorrected for aero-elastic and engine gyroscopic coupling effects, as these effects are quite small at high altitude.

9 COMPARISON WITH EXPERIMENTAL AND THEORETICAL DATA FROM OTHER SOURCES

The results obtained from the flight tests at 38,000 ft altitude (without any corrections for aero-elasticity or engine gyroscopic coupling) have been compared in Figs.15, 18, 19 and 20 with data obtained from the following tests made on models representative of the full scale aircraft:

(a) Rocket model tests (Ref.7)

The results were obtained by exciting the longitudinal short period oscillation. The C.G. position was at 87 in. (full scale) aft of the wing apex. The tests were at zero incidence, a Reynolds number of about 10×10^6, and a reduced frequency of about 0.08.

The intake was not represented on the models tested.

(b) Wing flow tests (Refs.3 and 4)

A single degree of freedom free oscillation technique was used on a half model. Tests were made at a reduced frequency of 0.16 to 0.10 and at incidences of 0°, 2° and 5°. The Reynolds number was 0.8×10^6 and the axis of rotation was at 169 in. (full scale) aft of the wing apex. Static measurements of C_m and C_L were also made over a range of incidences. Transition fixers at 5% chord were used for the oscillatory tests, but not for the static tests.

The intake was represented by a solid fairing.

(c) High speed wind tunnel tests (Unpublished RAE Data)

Static measurements of C_L and C_m were made in the RAE 10 ft x 7 ft High Speed Wind Tunnel over a range of incidences at Mach numbers up to 0.94. The Reynolds number was 2×10^6. Transition was not fixed.

The intake and the flow through were represented.

(d) Supersonic wind tunnel tests (Unpublished RAE Data)

For comparison, the Reynolds number of the flight tests at 38,000 ft altitude was between 25×10^6 and 60×10^6 and the reduced frequency about 0.08.

Fig.21 shows a comparison between the flight test data and some theoretical estimates.

$\left(\frac{\partial C_L}{\partial \alpha}\right)_{M,\eta}$

Fig.18 shows that although the results from wing flow, rocket model, and subsonic wind tunnel tests agree amongst themselves, they are some 10% lower than the flight values. The supersonic wind tunnel results are in very good agreement with the flight results. Comparison is made with some theoretical estimates in Fig.21. At supersonic speeds, the theoretical lift curve slope for the wing alone is little different from that of the wing-body combination, and this is also true at low Mach number[14]. It is seen that agreement with the theoretical values is good at supersonic speeds, but there is a discrepancy of some 15% at subsonic speeds. However, it is probable that the flight data is not particularly accurate at Mach numbers below 0.9 due to the small number of experimental points and to the difficulty of measuring q^*/n^* accurately when only one or two cycles are available for analysis.

The degree of agreement obtained between the various experimental and theoretical data is considered generally satisfactory.

$m_{\dot{\theta}}$

Fig.19 shows that the wing flow results agree well with the flight results, both in magnitude and in predicting the loss of damping at M = 0.96. The rocket model tests give considerably larger values of $-m_{\dot{\theta}}$ because of the very far forward C.G. position used on the model to achieve the correct reduced frequency. The correction necessary to reduce this result to the full scale C.G. position is large and cannot be accurately estimated[7]. The rocket model results are seen to predict the fall in damping at M = 0.96 but for some reason show a second trough near M = 1.07 that is not present in the full scale results.

Theoretical estimates for the wing alone agree well with the flight measurements at subsonic speeds, but are somewhat larger at supersonic speeds (Fig.21).

m_w

Comparative values are shown in Fig.20, all results having been corrected to a C.G. position of 163 in. aft of the wing apex. In comparing the flight data with wing flow and subsonic wind tunnel results, it is useful to bear in mind that the flight C_L and incidence are 0.25 and 5° at 38,000 ft at M = 0.7, and 0.10 and 2° at M = 1.1. The wing flow and subsonic wind tunnel data are in good agreement with the flight results, but the rocket model and supersonic wind tunnel tests give values of $-m_w$ about 20% larger. A small amount of this discrepancy can be accounted for by aero-elastic effects (Fig.17). However, since this 20% difference amounts to only 0.03 in manoeuvre margin, the agreement is thought to be reasonably good, particularly when allowance is made for possible errors in the assumed value of i_B (para.6.2).

Agreement with theory for the wing alone is good at supersonic speeds (Fig.21). At subsonic speeds, the theoretical values of m_w are only about 50% of the measured values, although this discrepancy corresponds to only about 0.03 in manoeuvre margin. Body effects on the m_w for the wing alone are negligible [13,14].

m_η

The values of m_η obtained from wind tunnel tests are shown in Fig.15. The subsonic wind tunnel and the flight test results agree at low Mach number, but the rapid rise in $-m_\eta$ above M = 0.85 is not present in flight. The supersonic wind tunnel results are about 50% higher than the flight values, although this difference reduces to about 35% when the flight results are corrected for aero-elasticity (Fig.17). Discrepancies of this magnitude are not unexpected due to the poor accuracy in the determination of m_η from the flight test data and the possibility of error in the assumed value of i_B (para. 6.2).

10 COMPARISON OF THE MEASURED DAMPING WITH THE FLYING CHARACTERISTICS OF THE AIRCRAFT

In this paragraph an attempt is made to relate the measured longitudinal damping to the flying characteristics of the aircraft. In so doing, it is important to remember that pilots' impressions are coloured not only by the aerodynamic damping present, but also by the quality and effectiveness of the longitudinal control system. Characteristics which are known to be due solely to deficiencies in the longitudinal control system are not discussed here.

Pilots have complained of a region of poor longitudinal damping near M = 0.95, making the aircraft difficult to control. This is particularly apparent when manoeuvring at this speed. The damping is otherwise satisfactory for a research aircraft, although a military application would almost certainly require artificial damping in pitch.

During an approach to land in turbulent weather, the main difficulties arise from the lateral and directional characteristics, and the longitudinal damping seems adequate.

The pilot's complaint of poor damping near M = 0.95 might be expected from the "trough" in the aerodynamic damping (Fig.8). However, it is certain that much of the pilots' difficulty stems from oscillations induced by the pilot in attempting to fly in the nose-down trim change that also occurs in this speed range.

11 CONCLUSIONS

Longitudinal short period oscillations were excited in flight on the Fairey Delta 2 aircraft by stick pulses. Using the technique of Ref.2, the longitudinal derivatives were obtained by analysing that part of each oscillation where the elevator position was sensibly constant.

(1) The results obtained at 38,000 ft altitude showed that

(i) the lift curve slope increased to a peak value of 3.7 at M = 1.0, thereafter falling off progressively and reaching 2.4 at M = 1.56,

(ii) although the total damping of the aircraft was always positive, the rotary damping derivative $m_\dot{\theta}$ became destabilising over a small band of Mach number near M = 0.96.

(iii) the manoeuvre margin, H_m, increased from 0.08 to 0.12 at transonic speeds and then continued to increase at a slower rate with increasing supersonic Mach number,

(iv) $-m_w$ increased rapidly from 0.12 at M = 0.9 to a maximum of 0.21 at M = 0.96 and then decreased very slowly with further increase in Mach number,

(v) the elevator effectiveness, m_η, decreased rapidly as speed increased beyond M = 1.0. By M = 1.6, m_η had fallen to about a third of its subsonic value.

(2) Agreement between the flight test results at 38,000 ft altitude and the results of rocket model, wing flow, and wind tunnel tests was generally satisfactory.

(3) The values of $\partial C_L/\partial\alpha$, H_m and $-m_w$ obtained at 10,000 ft altitude were appreciably lower than the values obtained at 38,000 ft. This difference can be explained by aero-elastic effects and by the possible effects of elevator oscillations small enough to be within the resolution of the instrumentation recording elevator movement and therefore undetectable.

(4) In view of the possibility of errors in the derivatives arising from an error in the estimated value of i_B, measurements of this quantity are required on the full scale aircraft.

LIST OF SYMBOLS

$a = \left(\frac{\partial C_L}{\partial \alpha}\right)_{M,\eta}$ = lift curve slope at constant Mach number and constant elevator angle

A = inertia in roll

B = inertia in pitch

C = inertia in yaw

$\bar{c}$ = mean aerodynamic chord (16.75 ft)

$C_p = \frac{p_{indic} - p_{true}}{\frac{1}{2}\rho V^2}$

g = acceleration due to gravity (32.2 ft/sec^2)

H_m = manoeuvre margin stick fixed

LIST OF SYMBOLS (Contd.)

i_B = non-dimensional moment of inertia in pitch = $\dfrac{\text{inertia in pitch}}{W \bar{\bar{c}}^2}$

$\mathcal{J}$ = frequency = $\dfrac{2\pi}{P}$

J = dimensionless frequency of short period oscillation = $\mathcal{J} \hat{t}$

$\bar{J}$ = dimensionless frequency of short period oscillation, control fixed (see Appendix 2)

K_n = restoring margin = $-\dfrac{\partial C_m}{\partial C_L}$

ℓ = distance of normal accelerometer ahead of C.G. (ft)

m_q = steady rotary damping in pitch derivative = $\dfrac{M_q}{\rho S V \bar{\bar{c}}^2}$

m_w = pitching moment derivative due to w = $\dfrac{M_w}{\rho V S \bar{\bar{c}}} = \dfrac{1}{2}\dfrac{\partial C_m}{\partial \alpha}$

$m_{\dot{w}}$ = pitching moment derivative due to $\dot{w}$ = $\dfrac{M_{\dot{w}}}{\rho S \bar{\bar{c}}^2}$

m_η = pitching moment derivative due to elevator angle for constant C_L = $\dfrac{1}{2}\dfrac{\partial C_m}{\partial \eta}$

$m_{\dot{\vartheta}}$ = full rotary damping derivative = $\dfrac{M_{\dot{\vartheta}}}{\rho S V \bar{\bar{c}}^2}$

m_β = pitching moment derivative due to sideslip angle

M = Mach number of aircraft

n = excess normal acceleration (= load factor minus one) g units

n_{indic} = apparent excess normal acceleration registered by accelerometer displaced from C.G.

p = $\dfrac{V}{g}\dfrac{q^*}{n^*}$ also static pressure

LIST OF SYMBOLS (Contd.)

$\left(\frac{q^*}{n^*}\right)_{indic}$ = $\left(\frac{q^*}{n^*}\right)'$ corrected for instrument phase lag

$\left(\frac{q^*}{n^*}\right)$ = value of $\left(\frac{q^*}{n^*}\right)_{indic}$ corrected for accelerometer being ahead of C.G.

$\mathcal{R}$ = $\frac{1}{2}(\mathcal{R}_q + \mathcal{R}_n)$

$\mathcal{R}_q$ = damping factor of rate of pitch oscillation = $\frac{d(\log_e q)}{dt}$

$\mathcal{R}_n$ = damping factor of normal acceleration oscillation

R = $\mathcal{R}\,\hat{t}$

S = wing area of aircraft

$\hat{t}$ = aerodynamic time = $\frac{W}{\rho g S V}$

V_i = EAS ft/sec

V = true airspeed ft/sec

ω = reduced frequency $\left(= \frac{2\pi\,\bar{\bar{c}}}{VP}\right)$ also vertical velocity

W = weight of aircraft (lb)

α = angle of incidence of wing

Δ = $\frac{\pi}{2} - \phi_{qn}$

ϕ'_{qn} = phase angle by which q leads n (indicated value)

ϕ_{qn} = ϕ'_{qn} corrected for instrument phase lag

$\phi_{\eta n}$ = phase angle by which η leads n

χ = angle by which phase lag of rate gyro exceeds that of normal accelerometer

η = elevator angle

μ = $\frac{W}{\rho g S \bar{\bar{c}}}$

ρ = ambient air density (slugs/ft^3)

LIST OF REFERENCES

No.	Author	Title, etc.
1	Rogers, E.W.E.	The effects of incidence on two Mk.9A pitot-static heads at subsonic speeds. ARC 18489. June 1956.
2	Neumark, S.	Analysis of short period longitudinal oscillations of an aircraft: Interpretation of flight tests. A.R.C. R.& M.2940 September, 1952
3	Shaw, M.M., Rose, R.	Wing flow measurements of lift and pitching moment at transonic speeds on a 60° delta (ER.103). Unpublished RAE Data. Dec. 1952.
4	Rose, R.	Wing flow measurements of the damping in pitch and stiffness derivatives of a 60° delta wing-body combination. Unpublished M.O.A. Report
5		Interim report on the longitudinal trim and manoeuvring characteristics of the Fairey Delta 2 (ER.103/49). Fairey Aviation Co. Flight Analysis Report No.V1.
6	McCarter, W.B.	Longitudinal stability characteristics and damping in pitch of delta wings. College of Aeronautics Note No.11. July 1954. ARC 18131.
7	Turner, K.J.	Free flight model measurements of the zero lift drag, longitudinal stability and rolling characteristics of a supersonic research aircraft (ER.103) over the Mach number range 0.8 to 1.4. Unpublished M.O.A. Report
8	Fry, D.E.	Theoretical analysis of the effect of engine gyroscopic coupling on the lateral and longitudinal motions of aircraft. RAE Report to be published.
9	Stanbrook, A.	The lift-curve slope and aerodynamic centre position of wings at subsonic and supersonic speeds. Unpublished M.O.A. Report
10	Mangler, K.W.	The short period longitudinal stability derivatives for a delta wing at supersonic speeds. Unpublished M.O.A. Report
11	Garner, H.C.	Multhopp's subsonic lifting surface theory of wings in slow pitching oscillations. A.R.C. R. & M. 2885 July, 1952
12	Mangler, K.W.	Effect of taper on the short period longitudinal stability derivatives of a delta wing in transonic flow. Unpublished M.O.A. Report

LIST OF REFERENCES (Contd)

No.	Author	Title etc.
13	Pitts, W.C., Neilsen, J.N., Kaattari, G.E.	Lift and centre of pressure of wing-body-tail combinations at subsonic, transonic and supersonic speeds. N.A.C.A. Report 1307 1957
14	Nonweiler, T.	Theoretical stability derivatives of a highly swept delta wing and slender body combination. College of Aeronautics Report No.50. Nov. 1951

APPENDIX 1

CORRECTION TO $\frac{q^*}{n^*}$ DUE TO NORMAL ACCELEROMETER NOT BEING AT THE C.G.

Let ℓ be the distance of the normal accelerometer ahead of the C.G. Then, using the notation of Ref.2, the indicated value of n is given by

$$n_{indic} = n^* e^{-\mathcal{R}(t-t_o)} \sin \mathcal{J}(t-t_o) + \frac{\ell}{g}\dot{q} \qquad (11)$$

and

$$q = q^* e^{-\mathcal{R}(t-t_o)} \sin [\mathcal{J}(t-t_o) + \phi_{qn}] . \qquad (12)$$

If we put $\Delta = \frac{\pi}{2} - \phi_{qn}$ and assume Δ is small, we have after reduction

$$n_{indic} = n^* e^{-\mathcal{R}(t-t_o)} \sin \mathcal{J}(t-t_o)$$

$$\times \left[1 + \frac{\ell}{g}\frac{q^*}{n^*}\left\{\Delta(-\mathcal{R} + \mathcal{J}\cot \mathcal{J}(t-t_o)) - (\mathcal{J} + \mathcal{R}\cot \mathcal{J}(t-t_o))\right\}\right]. \qquad (13)$$

By differentiating this expression and ignoring terms involving Δ, it can be shown that the peak values of n occur when

$$(\mathcal{R}^2+\mathcal{J}^2)\sin^2 \mathcal{J}(t-t_o) = \frac{\mathcal{J}^2 + \left\{\frac{\ell}{g}\frac{q^*}{n^*}(\mathcal{R}^2-\mathcal{J}^2)\right\}^2 + 2\mathcal{J}\frac{\ell}{g}\frac{q^*}{n^*}(\mathcal{R}^2-\mathcal{J}^2)}{1 + \left(\frac{\ell}{g}\frac{q^*}{n^*}\right)^2(\mathcal{R}^2+\mathcal{J}^2) - 2\mathcal{J}\frac{\ell}{g}\frac{q^*}{n^*}} .$$

We can with sufficient accuracy neglect $\mathcal{R}^2$ in comparison with $\mathcal{J}^2$, and this then becomes

$$\sin \mathcal{J}(t-t_o) = \pm \frac{\mathcal{J}}{\sqrt{\mathcal{R}^2+\mathcal{J}^2}} .$$

Again ignoring terms involving Δ and neglecting $\mathcal{R}^2$ in comparison with $\mathcal{J}^2$, consecutive peaks of the curve (13) are

$$n_{1_{indic}} = n^* e^{-\mathcal{R}(t_1 - t_o)} \frac{\mathcal{I}}{\sqrt{\mathcal{R}^2 + \mathcal{I}^2}} \left[1 - \mathcal{I} \frac{\ell}{g} \frac{q^*}{n^*}\right]$$

corresponding to $t_1 = t_o + \frac{1}{\mathcal{I}} \tan^{-1} \frac{\mathcal{I}}{\mathcal{R}}$

$$n_{2_{indic}} = n^* e^{-\mathcal{R}(t_2 - t_o)} \frac{\mathcal{I}}{\sqrt{\mathcal{R}^2 + \mathcal{I}^2}} \left[1 - \mathcal{I} \frac{\ell}{g} \frac{q^*}{n^*}\right]$$

corresponding to $t_2 = t_o + \frac{\pi}{\mathcal{I}}$ etc.

Hence the ratio of the indicated peaks of n to the true peaks is

$$\frac{n_{indic}}{n} = \left[1 - \mathcal{I} \frac{\ell}{g} \frac{q^*}{n^*}\right]$$

$$\therefore \quad \frac{q^*}{n^*} = \left(\frac{q^*}{n^*}\right)_{indic} \left[1 - \mathcal{I} \frac{\ell}{g} \frac{q^*}{n^*}\right]$$

$$= \left(\frac{q^*}{n^*}\right)_{indic} \Big/ \left[1 + \mathcal{I} \frac{\ell}{g} \left(\frac{q^*}{n^*}\right)_{indic}\right]. \qquad (14)$$

Using expression (14), the indicated values of q^*/n^* can be corrected for the effect of the accelerometer not being at the C.G. This expression is approximate and depends upon ϕ_{qn} being almost $\pi/2$, $\mathcal{R}^2$ being small in comparison to $\mathcal{I}^2$, and ℓ small.

APPENDIX 2

EFFECT OF ELEVATOR MOVEMENT

In many cases it was found that some elevator motion occurred after the stick had returned to its trimmed position. This residual elevator motion was usually oscillatory in nature (Figs.6(b), (c) and (d)). Analysis of a record such as Fig.6(d) resulted in curved plots of log q and log n versus time, the damping being lowest when the elevator motion was largest. As no variations in the amplitude ratio q^*/n^* and the period were apparent, only the derivate $m_{\dot{\vartheta}}$ was affected by this elevator motion. A typical result at M = 1.2 to 1.5 at 40,000 ft was that $-m_{\dot{\vartheta}}$ was reduced by about 0.1 by the largest amount of elevator motion present. Necessarily approximate calculations using the method of Ref.2 combined with estimated values of m_η, z_η and m_q confirm the sign and general magnitude of this change in $m_{\dot{\vartheta}}$.

As a result of such findings only that part of each oscillation where the elevator motion was sensibly constant was analysed in presenting the results given in the main body of this report. However this does not of course preclude the possibility of small elevator motions within the resolution of the instrumentation recording elevator movement being present and modifying the characteristics of the longitudinal oscillation. The possible order of these effects will now be discussed.

The largest amplitude of elevator motion that could occur without being readily detected on the Hussenot trace is considered to be about $\pm 0.04^\circ$. The amplitude of n varies from about $\pm 1.0g$ to about $\pm 0.1g$ during the part of the oscillation that is usually analysed. Taking a mean value of 0.5g gives a ratio of η^*/n^* of 0.0014 radian. From the elevator motion that can be detected, the angle $\phi_{\eta n}$ by which the elevator angle leads the normal acceleration is about -150° at 40,000 ft and about 0° at 10,000 ft altitude. We will assume the same phase angles for the motion that is undetectable. By neglecting the effect of z_η and using the values of m_η given in Fig.15 we have[2]

Altitude	M	$\phi_{\eta n}$	ΔR	$-\Delta m_{\dot{\vartheta}}$	$\frac{\bar{J}}{J}$
40,000 ft	0.7	-150°	0.039	0.013	1.01
	0.9		0.063	0.023	1.01
	1.0		0.073	0.027	1.01
	1.2		0.044	0.018	1.00
	1.6		0.042	0.017	1.00
10,000 ft	0.7	0	0	0	0.90
	1.0		0	0	0.92
	1.2		0	0	0.95

In the above table, ΔR and $\Delta m_{\dot{\vartheta}}$ are the corrections necessary to correct the results to elevator fixed conditions. The elevator fixed non-dimensional frequency is $\bar{J}$. With the values of $\phi_{\eta n}$ assumed it will be seen that the errors in $m_{\dot{\vartheta}}$ are only 0.03 or less. As a and H_m are approximately proportional to J and m_w to J^2, the errors in these derivatives, although small at 40,000 ft, become appreciable at 10,000 ft. Thus at 10,000 ft at M = 1.0 the values of a and H_m may be too high by 8% and the value of $-m_w$ too high by 16%. But this

is of the opposite sign to the altitude effect shown by the flight test results, and leads one to suspect the values of $\phi_{\eta n}$ assumed above.

The value of $\phi_{\eta n}$ measured at 40,000 ft was obtained from an oscillation of several cycles, whereas that at 10,000 ft was obtained from only half a cycle and may therefore be considerably in error. If we assume that $\phi_{\eta n}$ is the same at 10,000 ft as at 40,000 ft then the effect of elevator motion at 10,000 ft is as follows:-

Altitude	M	$\phi_{\eta n}$	ΔR	$-\Delta m_{\vartheta}$	$\frac{\bar{J}}{J}$
10,000 ft	0.7	-150°	0.400	0.10	1.20
	1.0		0.535	0.17	1.17
	1.2		0.343	0.11	1.10

The errors in J are now of the right sign and approximately the right magnitude to explain the altitude effect found in a, H_m and m_w. The errors in m_{ϑ}, although large, are not significant in relation to the experimental errors associated with the measurement of this derivative at low altitude.

From the above discussion it would appear that

(1) unless the resolution of the elevator trace is very high, large errors can result at low altitude from small undetected elevator oscillations,

(2) the variations in m_w, H_m and a with altitude found in the present series of tests could be largely explained by the presence of small undetectable elevator oscillations if $\phi_{\eta n} = -150^{\circ}$ or thereabouts.

APPENDIX 3

ENGINE GYROSCOPIC COUPLING

The lateral and longitudinal motions of an aircraft are coupled to some extent by engine gyroscopic effects. This results in a change in the frequency and damping of the longitudinal short period oscillation, and also a distortion arising from a superimposed small amplitude oscillation of the same frequency as the lateral motion.

The change in frequency and damping have been calculated using the stability quartic (Ref.8) and the following results were obtained:

Altitude	M	Without coupling		With coupling		% Error due to gyroscopic coupling	
		P	$\mathcal{R}$	P	$\mathcal{R}$	$\frac{\Delta P}{P} \times 100$	$\frac{\Delta \mathcal{R}}{\mathcal{R}} \times 100$
40,000 ft	0.80	1.955	0.640	1.91	0.630	-2.3	-1.6
	0.93	1.44	0.995	1.42	0.986	-1.4	-0.9
	0.955	1.22	0.277	1.21	0.281	-1.0	1.4
	1.0	1.105	0.725	1.099	0.722	-0.6	-0.4
	1.2	0.941	0.657	0.936	0.657	-0.5	0
	1.4	0.825	0.741	0.825	0.744	0	0.4
	1.6	0.750	0.809	0.748	0.812	-0.3	0.4
10,000 ft	0.80	1.32	0.754	1.33	0.786	-0.8	4.1
	0.93	0.916	3.29	0.915	3.27	-0.1	-0.6
	0.955	0.861	0.711	0.854	0.736	-0.8	3.4
	1.0	0.722	2.12	0.717	2.10	-0.7	-1.0

The percentage error in period is seen to be generally quite small, and the effect of engine gyroscopic coupling is to make the measured values of a and H_m too high by up to 2% and that of $-m_w$ too high by up to 5% (see para.6). The errors are a maximum at low speed and high altitude.

The errors in $\mathcal{R}$ are negligible and result in errors in m_v of 0.01 or less.

TABLE 1

Details of Fairey Delta 2, Serial No. WG.777

Wing		
Gross area		360 sq ft
Span		26 ft 10 in.
Aspect ratio		2.00
Nominal centreline chord		25 ft 0 in.
Tip chord		1 ft 10 in.
Mean aerodynamic chord		16.75 ft
Standard mean chord		13 ft 5 in.
Wing section	4% symmetrical.	Max. t/c at 29.5% c
Leading edge sweepback		59.92°
Trailing edge sweepback		0°
Twist		0°
Dihedral		0°
Setting to fuselage datum		+ 1½°
C.G. datum position		240" forward of T.E.
Elevators		
Spanwise limits inboard		2 ft 0.2 in.
outboard		7 ft 6.0 in.
Chord inboard		4 ft 1.9 in.
outboard		3 ft 2.6 in.
Net area (one elevator)		20.22 sq ft
Angular movement (measured chordwise)		20° up
		33° down
Ailerons		
Spanwise limit inboard		7 ft 6.0 in.
outboard		13 ft 5.0 in.
Chord inboard		3 ft 2.6 in.
outboard		2 ft 2.5 in.
Net area (one aileron)		16.01 sq ft
Angular movement (measured chordwise)		±25°
Vertical tail		
Area (from 24" above fuselage datum)		37.4 sq ft
Height (from 24" above fuselage datum)		5 ft 6 in.
Rudder		
Limits - lower (above fuselage datum line)		0 ft 6.0 in.
upper (above fuselage datum line)		5 ft 6.0 in.
Chord - root		2 ft 7.9 in.
tip		0 ft 11.8 in.
Net area		9.1 sq ft
Angular movement (chordwise)		±22.1°
Fuselage		
Length (excluding pitot tube)		45 ft approx.

TABLE 1 (Contd)

Power plant

Engine	One Rolls Royce Avon RA28 with reheat and two position nozzle	
Rating	Static thrust at sea level	9600 lb
	Static thrust at sea level with reheat	13,000 lb

Weight and C.G.

(As flown for tests described in this report.)

All-up weight at take-off	13,840 lb
Fuel contents	306 galls
C.G. position at take-off, u/c down	105.9 in. aft of datum or 163.9 in. aft of L.E. of ℄ chord

Moment of inertia

The moment of inertia in pitch has been estimated by the Fairey Aviation Co. The following values correspond to a C.G. position at 165.3 in. aft of the L.E. of the centreline chord for undercarriage up.

Full fuel (13,800 lb A.U.W.)	798,000 lb ft^2
No fuel (11,300 lb A.U.W.)	646,000 lb ft^2

WT.2078.C.P.639.K3 - Printed in England

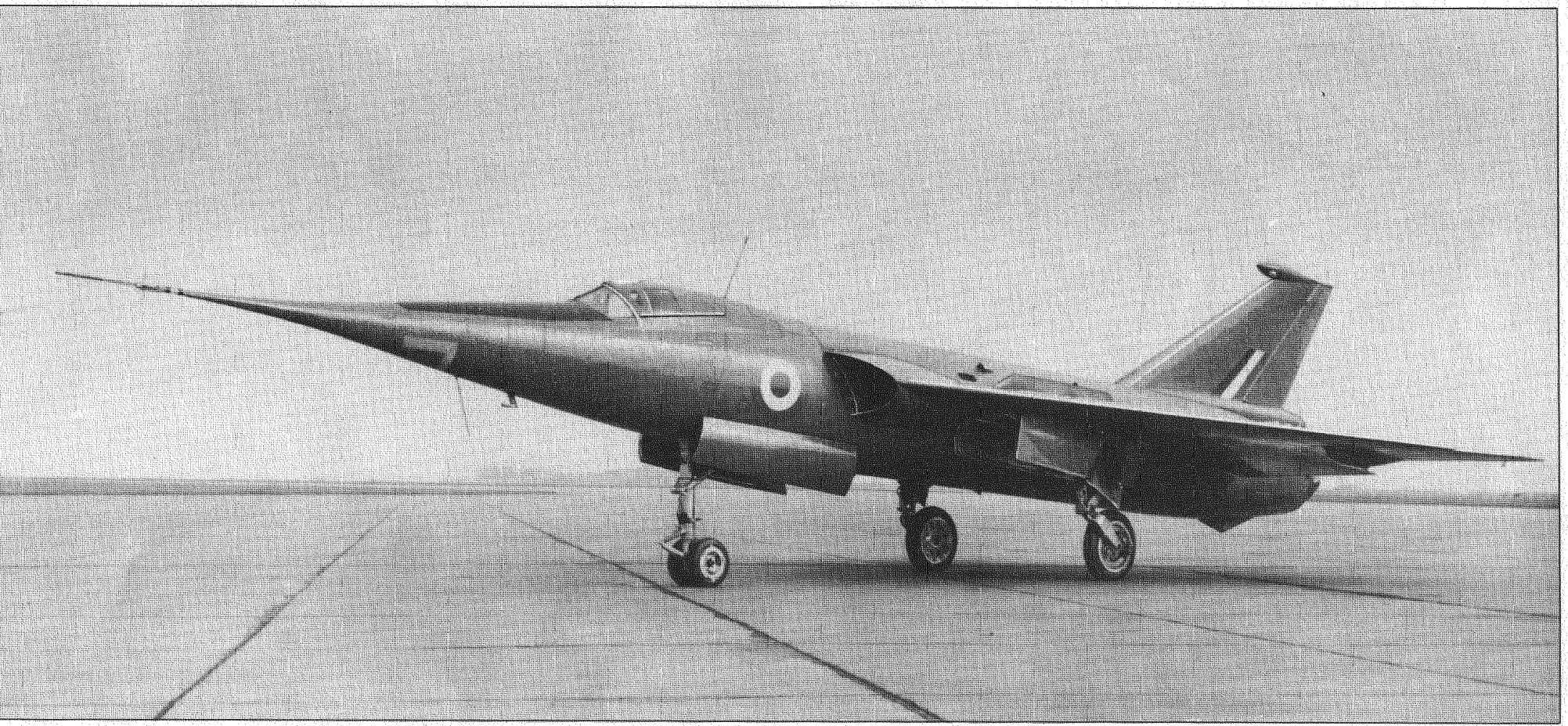

FIG.1. THE FAIREY DELTA 2 AIRCRAFT W.G. 777

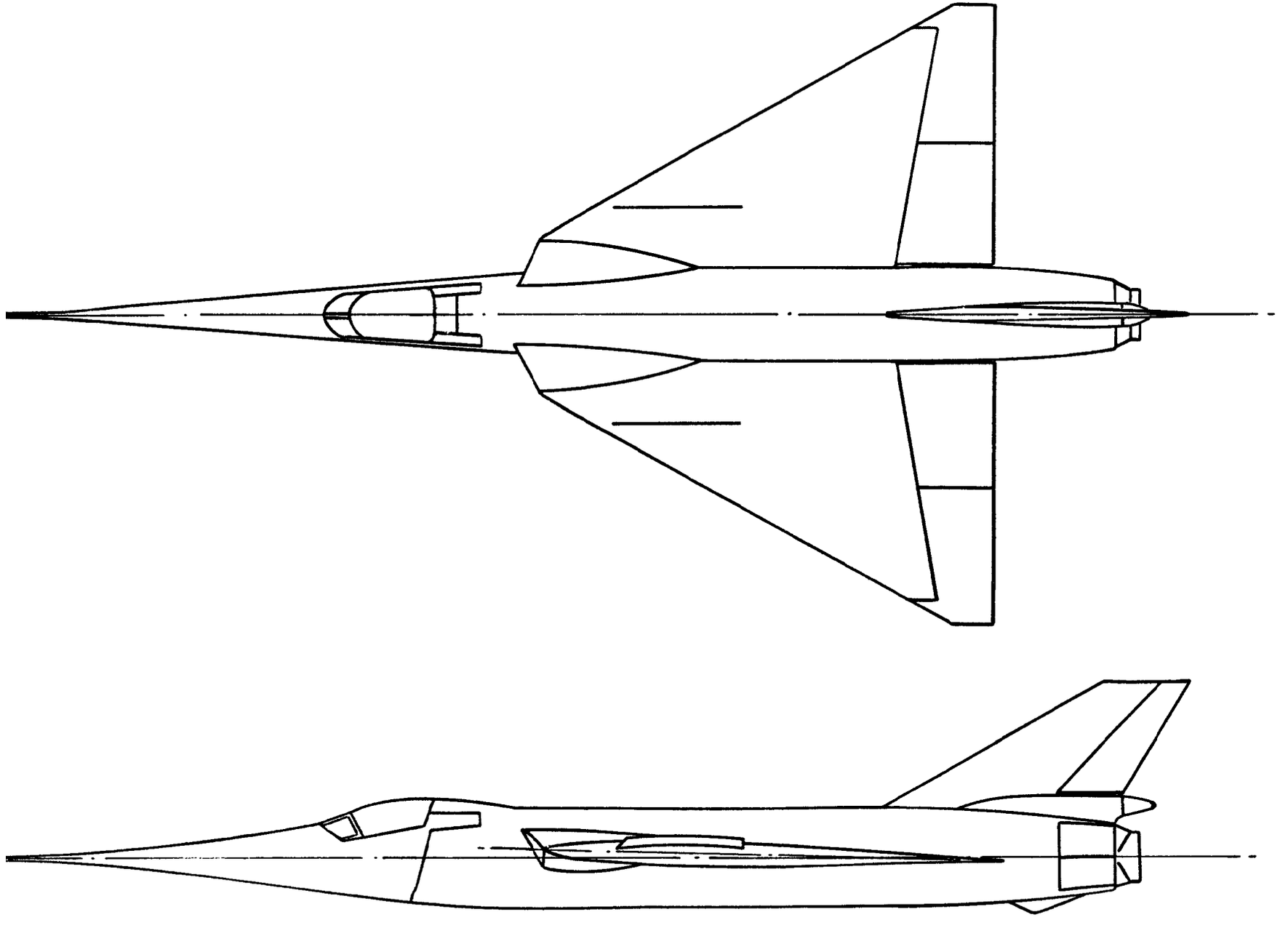

NERAL ARRANGEMENT OF THE FAIREY DELTA 2

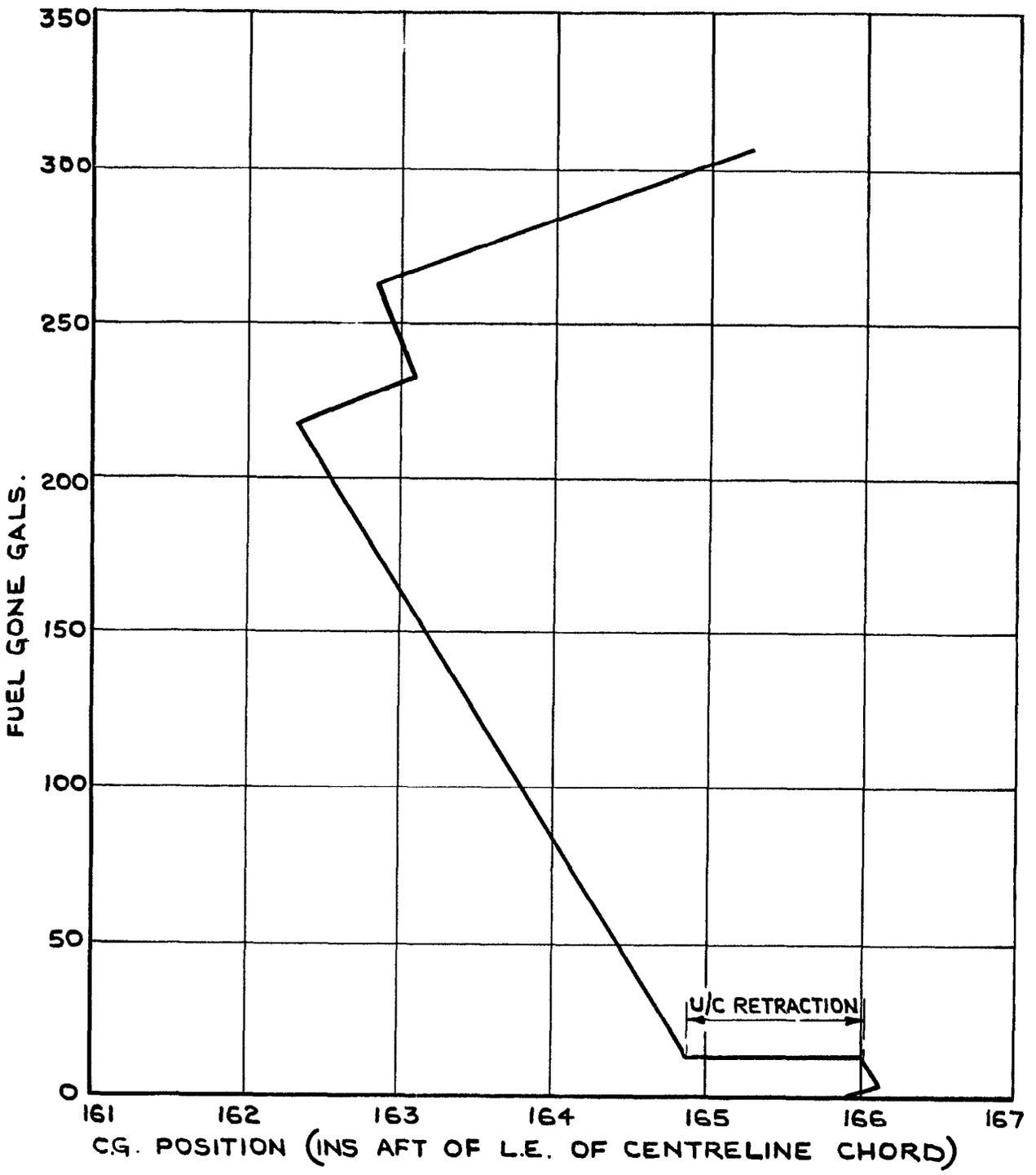

FIG.3 .VARIATION OF C.G. POSITION WITH FUEL CONTENTS DURING A TYPICAL FLIGHT.

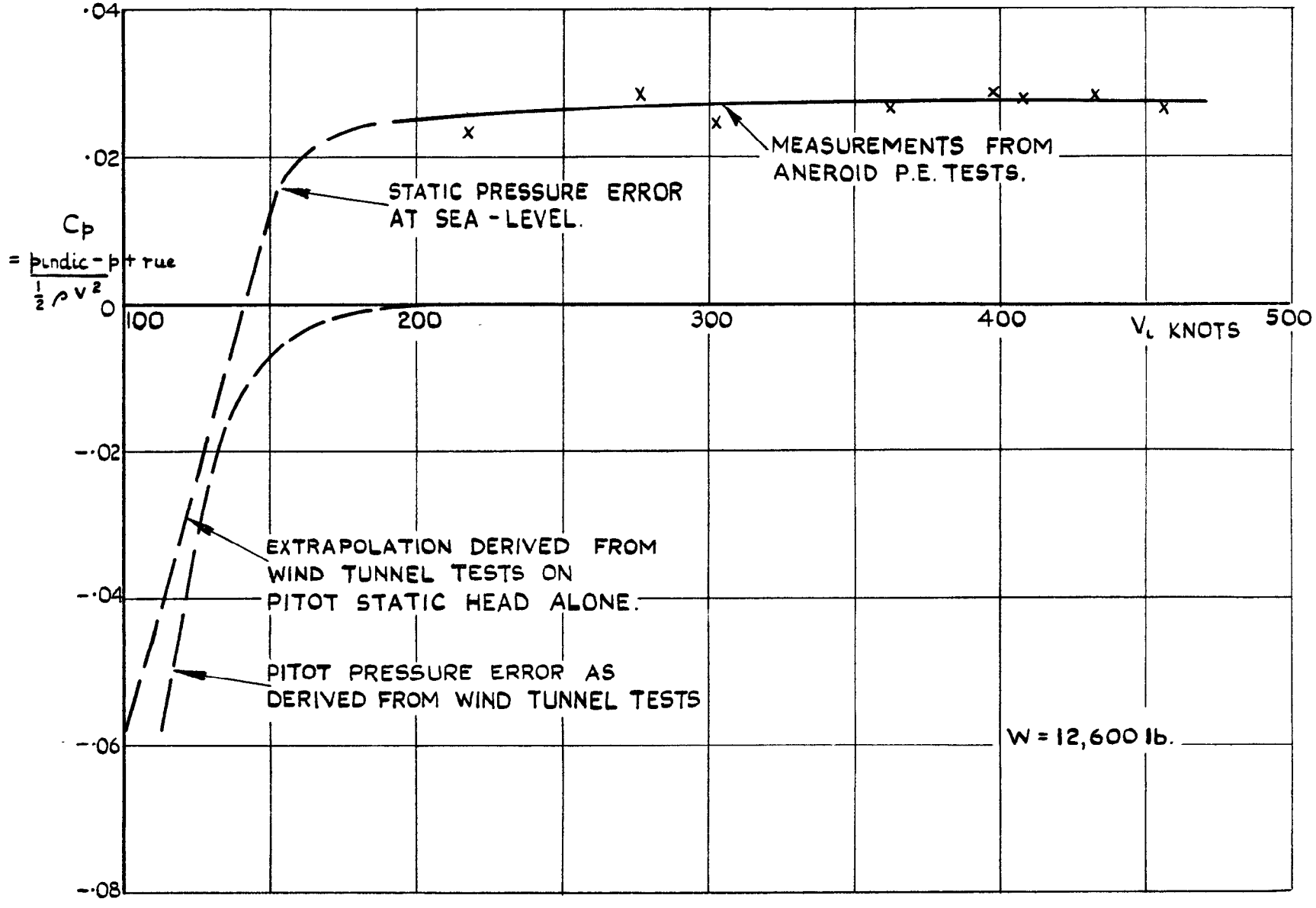

FIG. 4. FAIREY DELTA 2 W.G. 777 PRESSURE ERRORS AT SEA LEVEL.

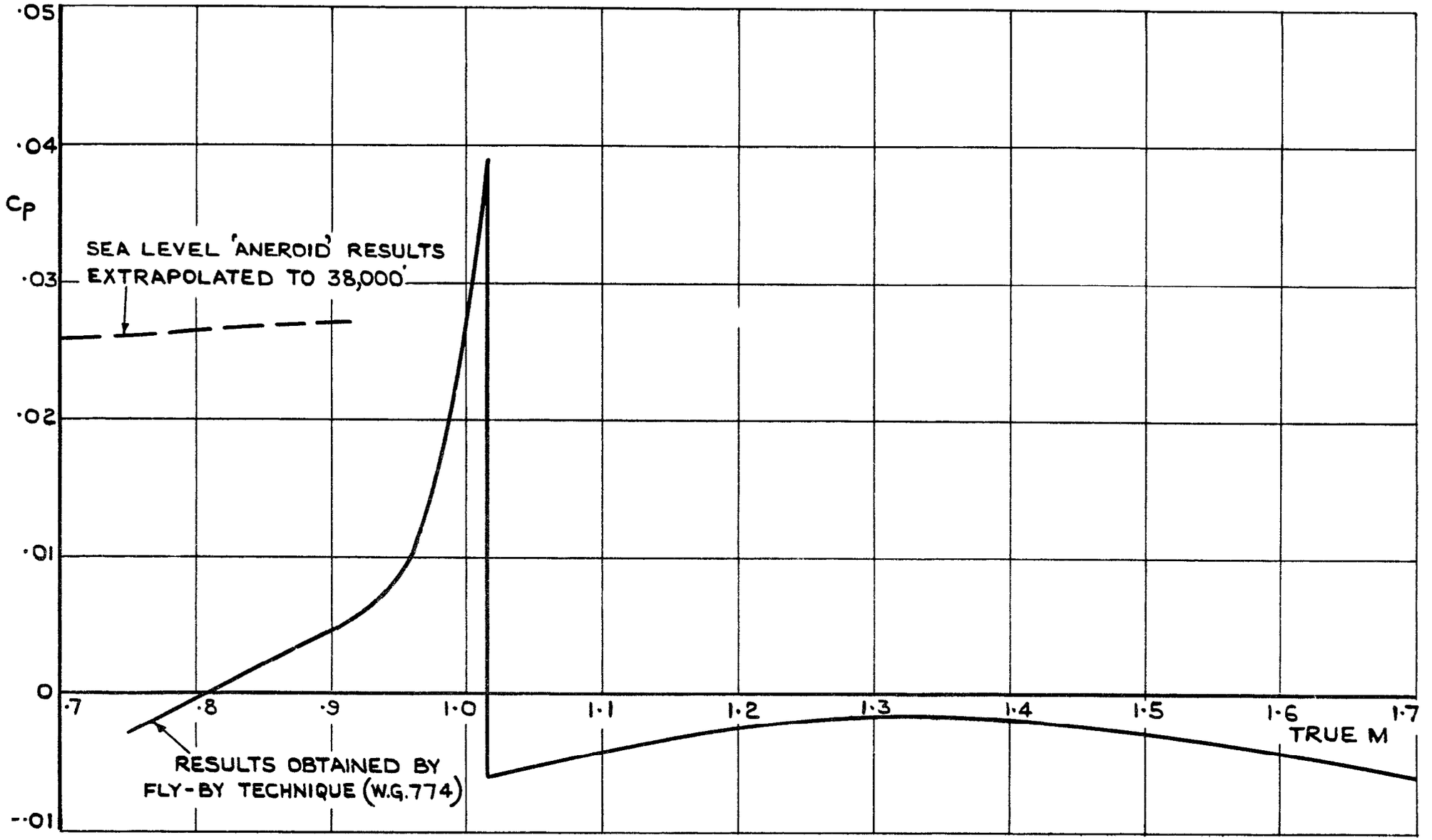

FIG. 5. COMPARISON OF STATIC P.E. DATA AT 38,000FT.

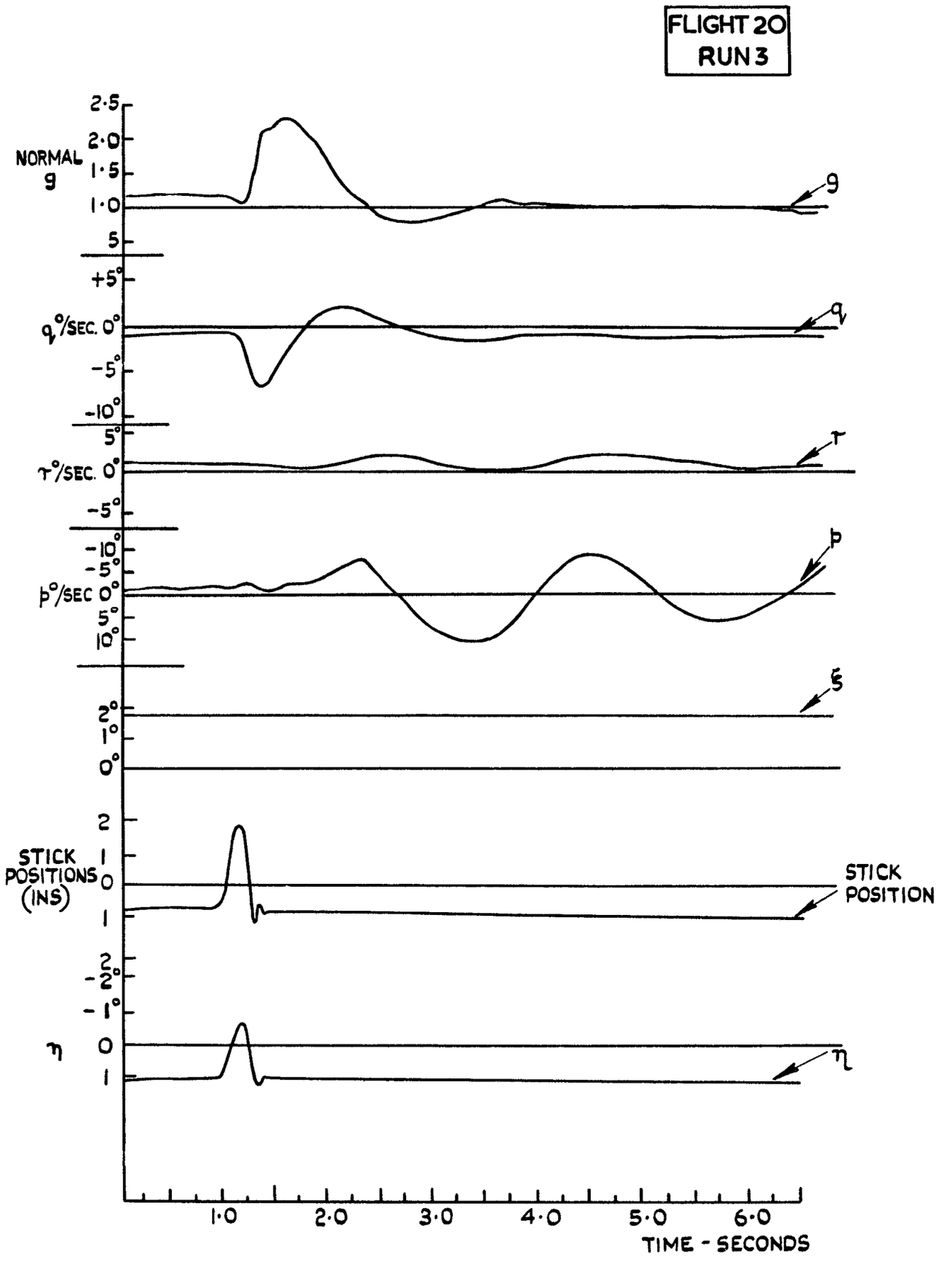
FLIGHT 20
RUN 3
NORMAL g
2·5
2·0
1·5
1·0
5
g
+5°
q°/SEC. 0°
-5°
-10°
q
5°
r°/SEC. 0°
-5°
r
-10°
-5°
p°/SEC 0°
5°
10°
p
ξ
2°
1°
0°
STICK POSITIONS (INS)
2
1
0
1
STICK POSITION
2
-2°
-1°
η
0
1
η
1·0
2·0
3·0
4·0
5·0
6·0
TIME - SECONDS

(a) M = 0·50 8500'

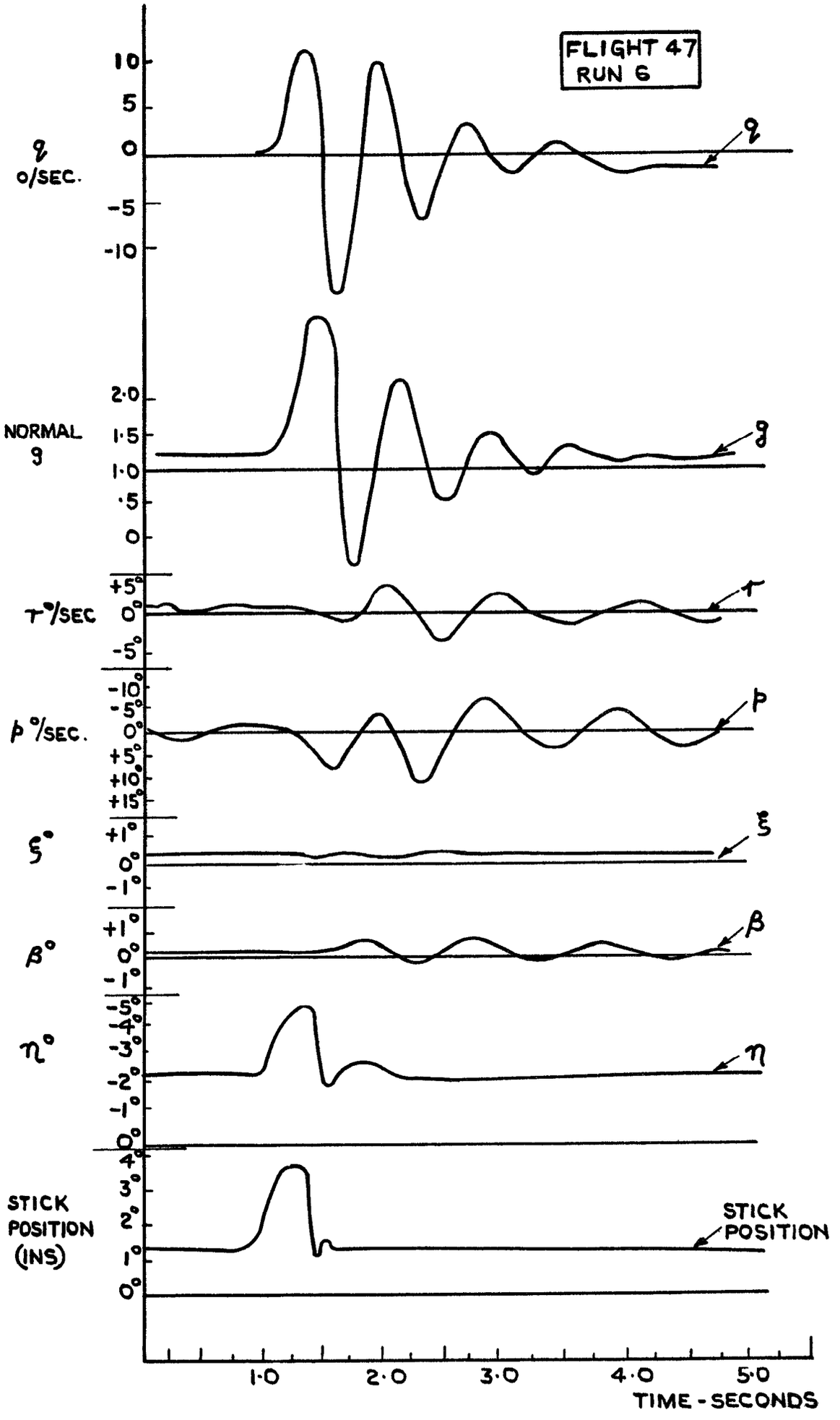

(b) M = 1·04 12,000'

FIG. 6(b). TIME HISTORY OF LONGITUDINAL SHORT PERIOD OSCILLATION.

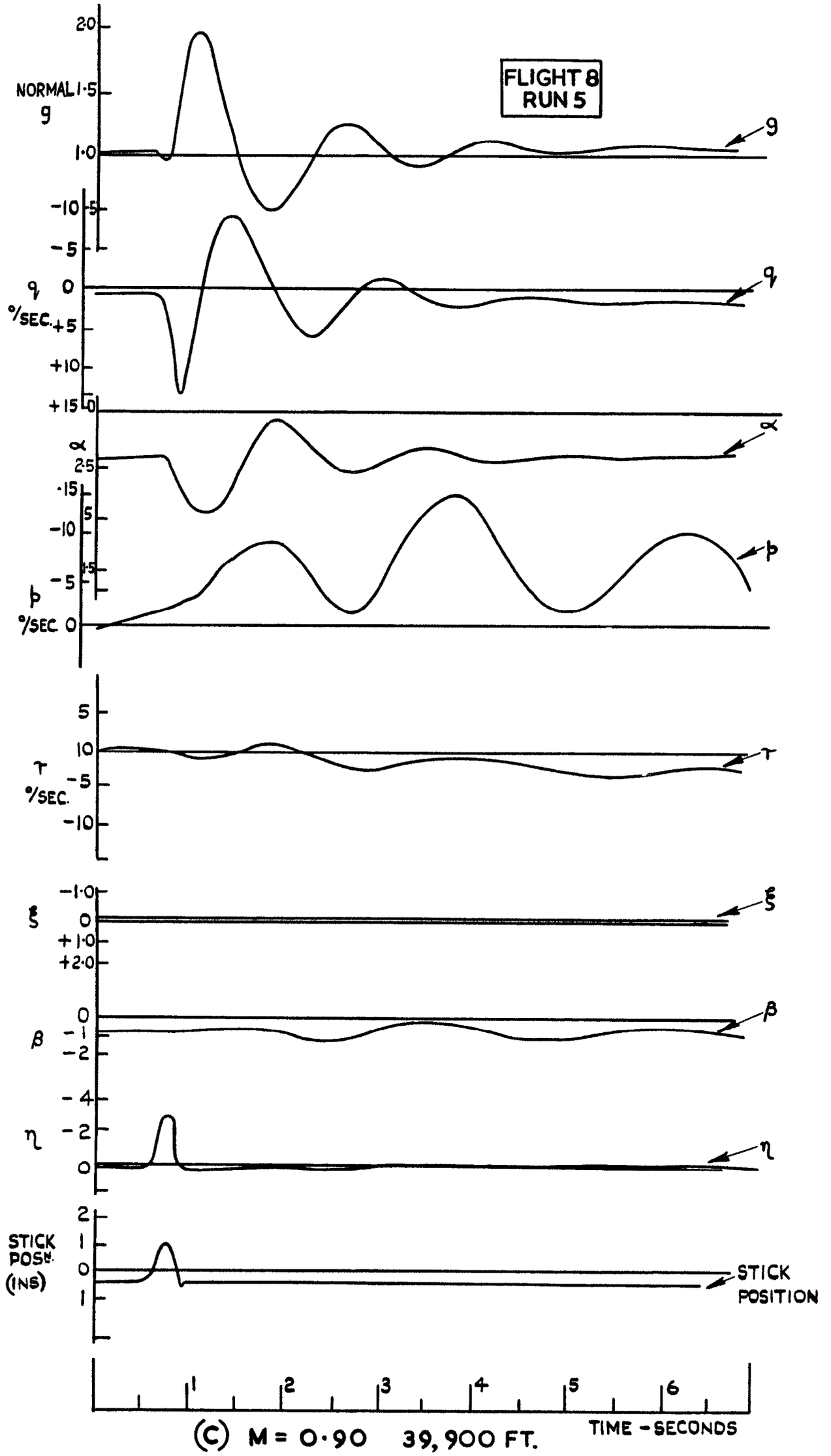

FIG. 6.(c). TIME HISTORY OF LONGITUDINAL SHORT PERIOD OSCILLATION.

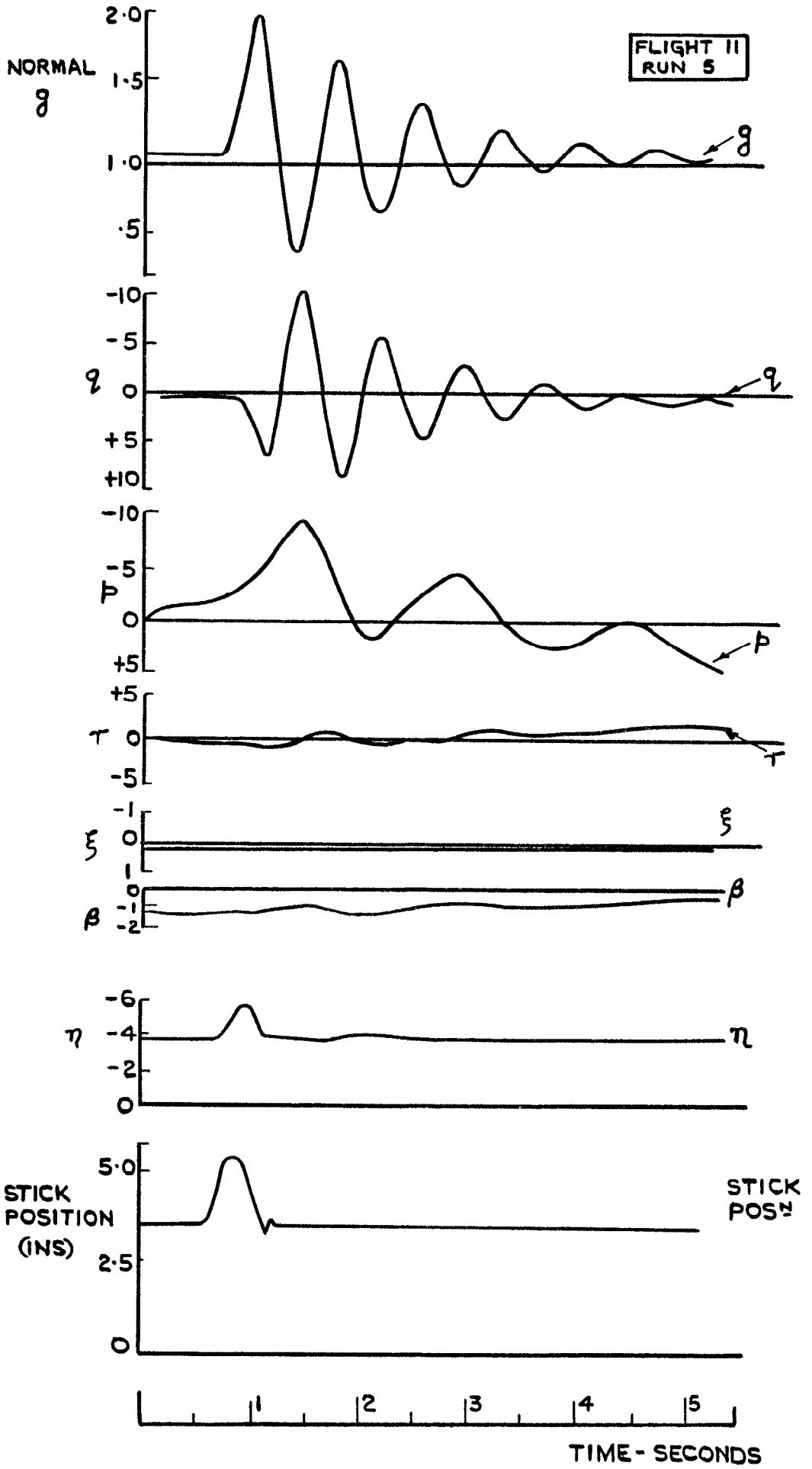

(d). M = 1·43, 35,600 FT.

FIG. 6(d). TIME HISTORY OF LONGITUDINAL SHORT PERIOD OSCILLATION.

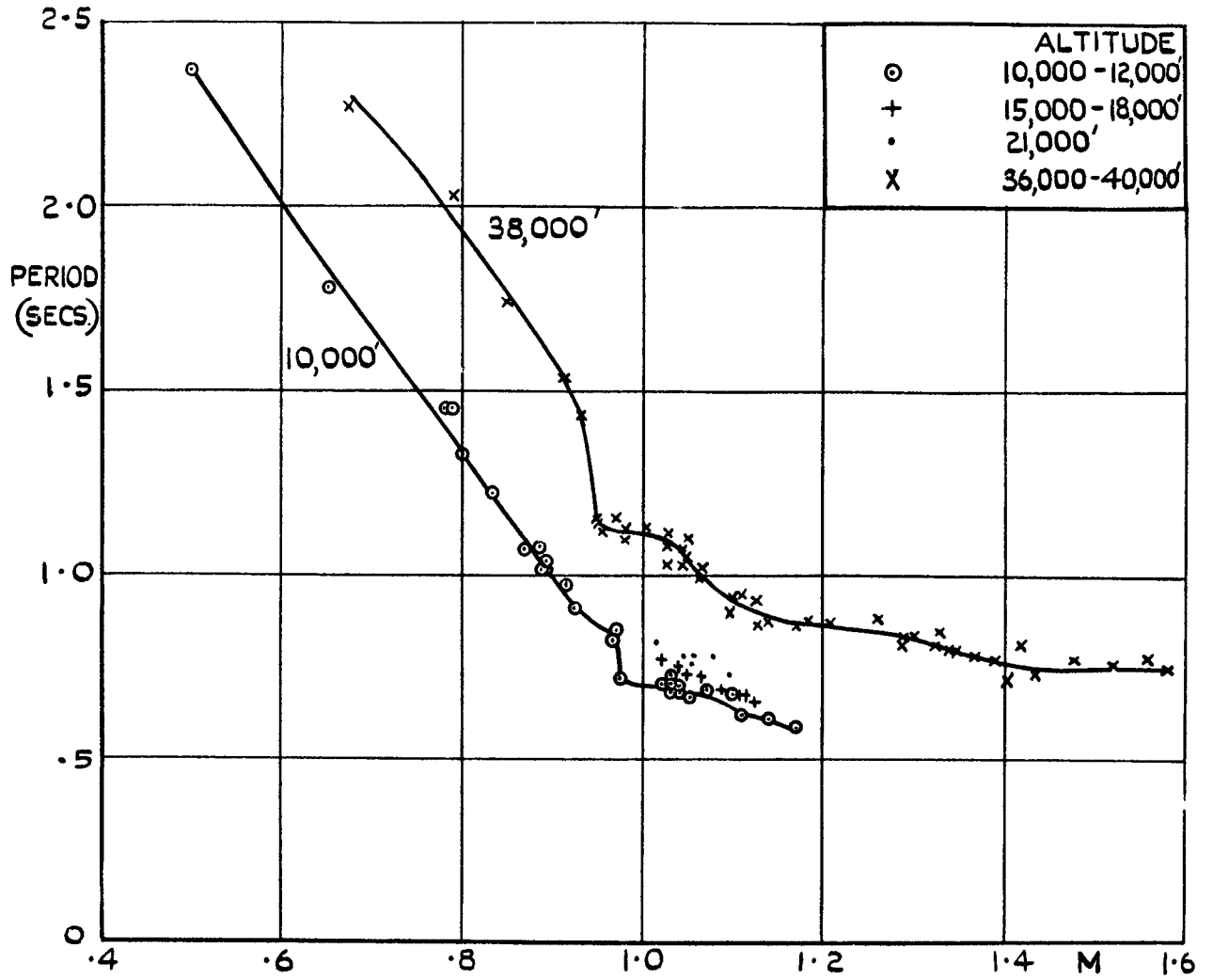

FIG. 7. PERIOD OF LONGITUDINAL OSCILLATIONS.

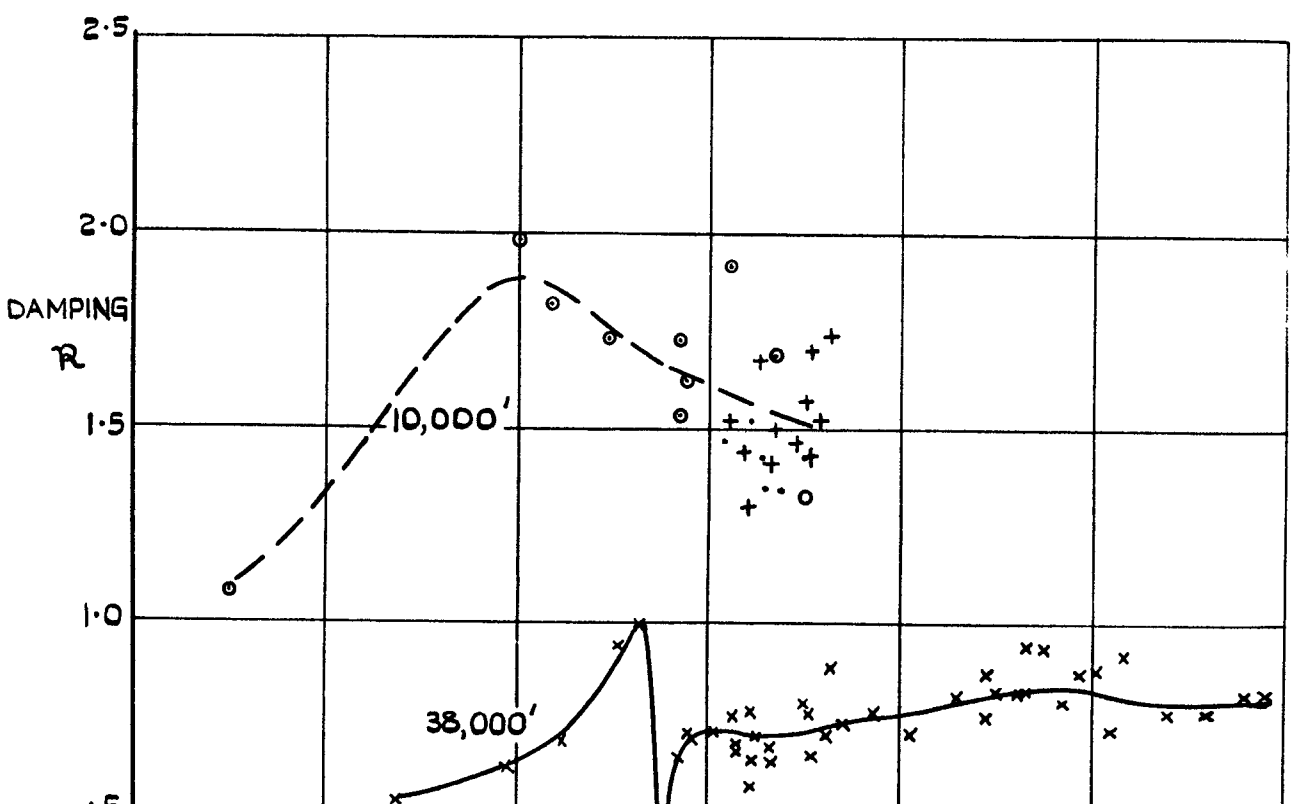

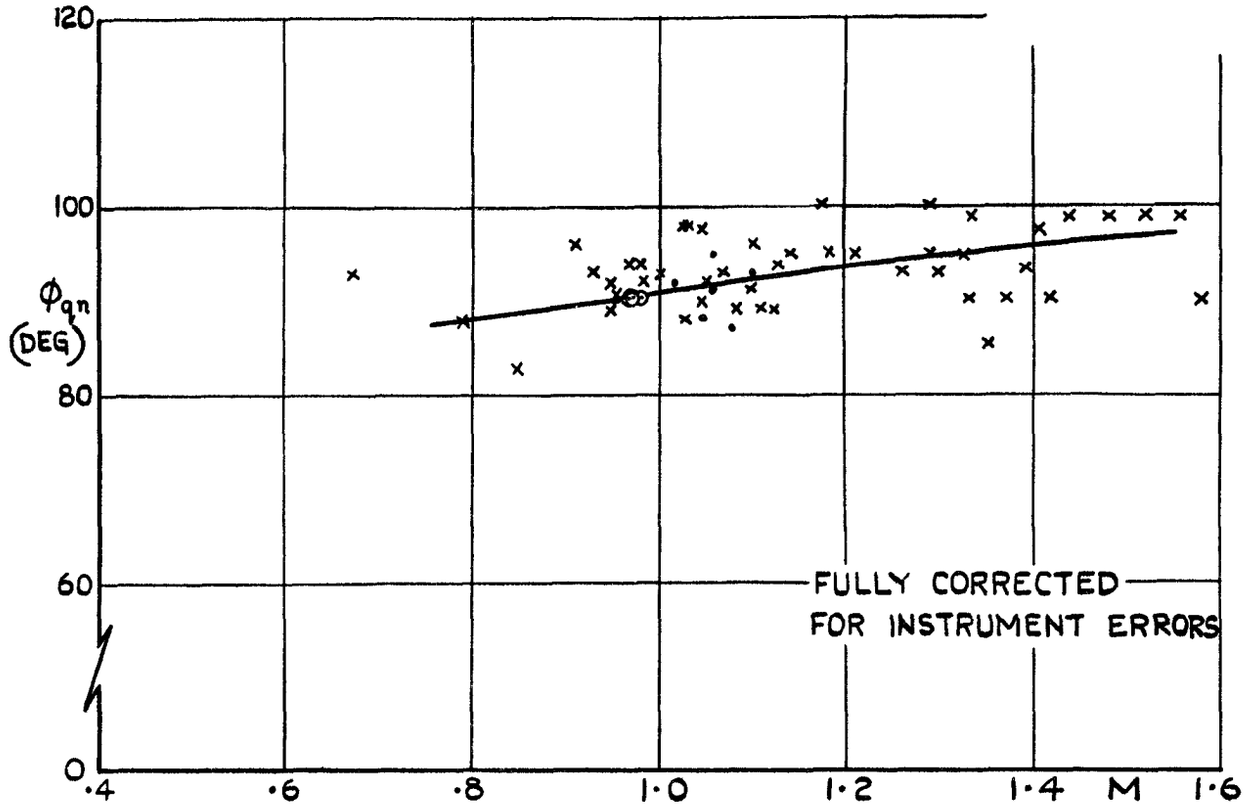

FIG. 9. PHASE ANGLE BY WHICH OSCILLATION OF q LEADS THAT OF n.

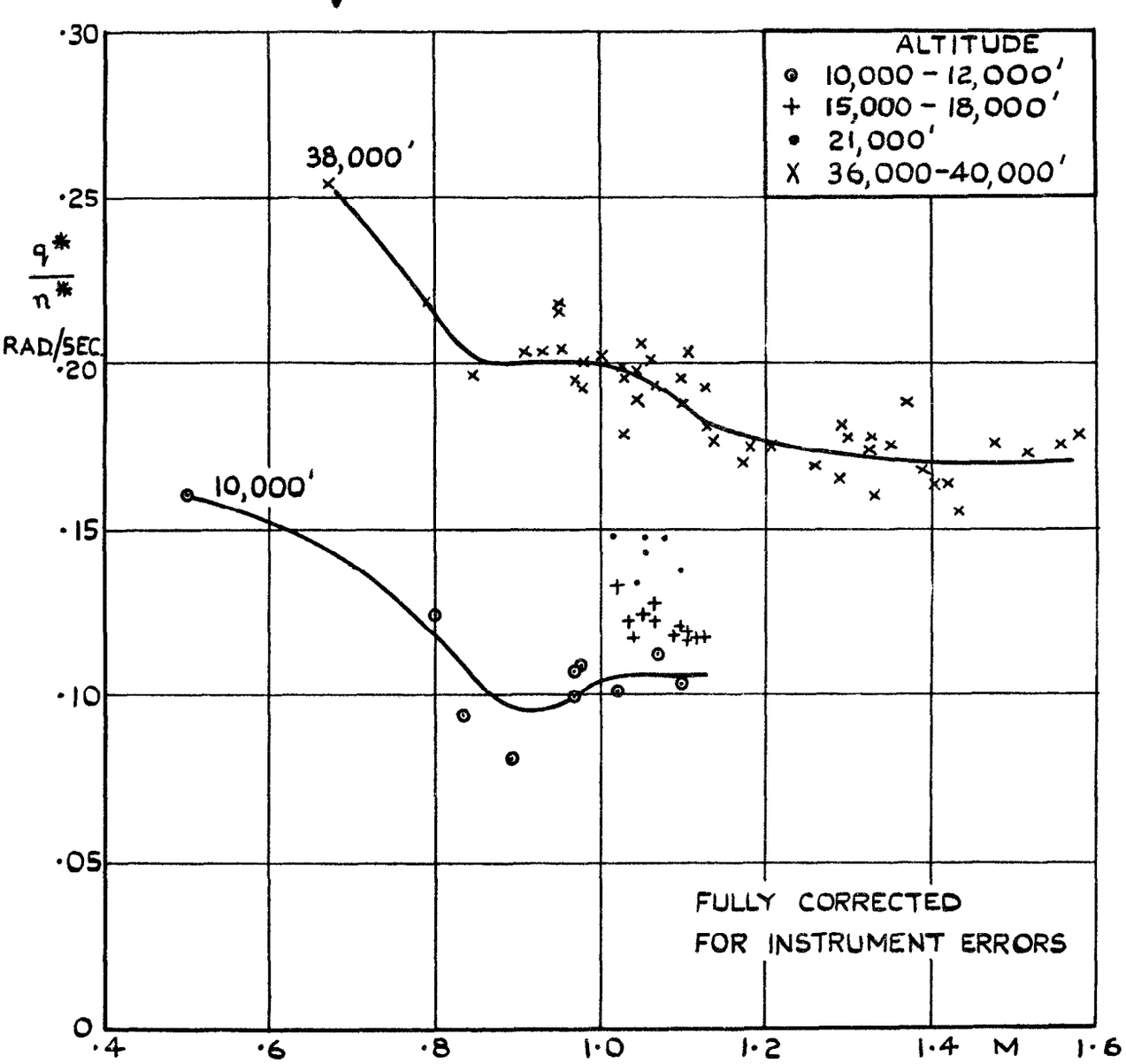

FIG. 10. AMPLITUDE RATIO OF q TO n.

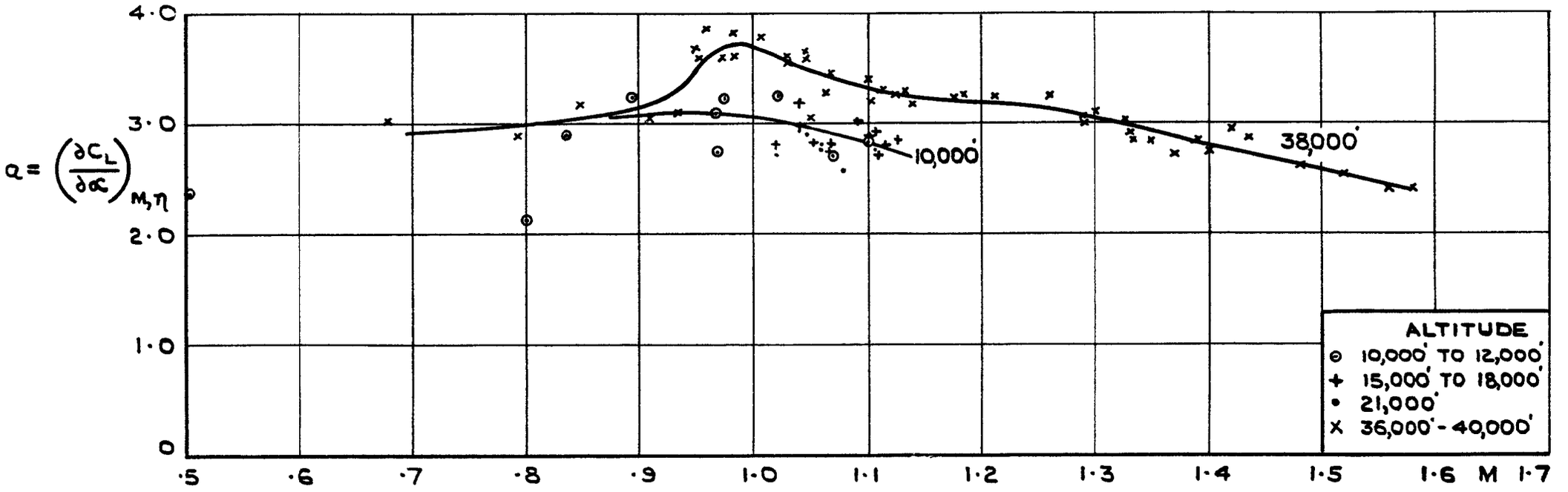

FIG.11 .VALUES OF LIFT CURVE SLOPE DERIVED FROM FLIGHT TESTS.

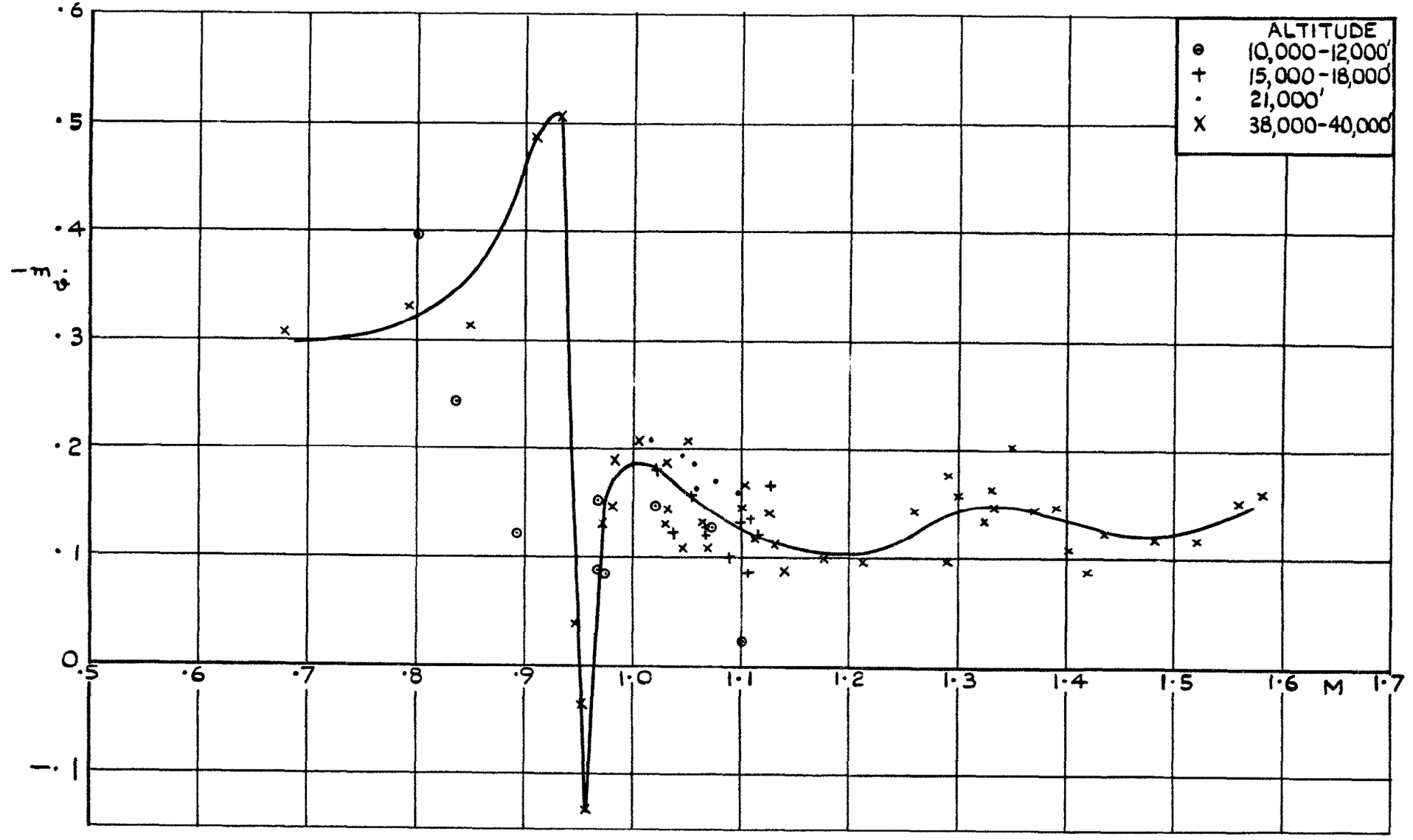

FIG. 12. ROTARY DAMPING DERIVATIVE $m_{\dot{v}}$ DERIVED FROM FLIGHT TESTS.

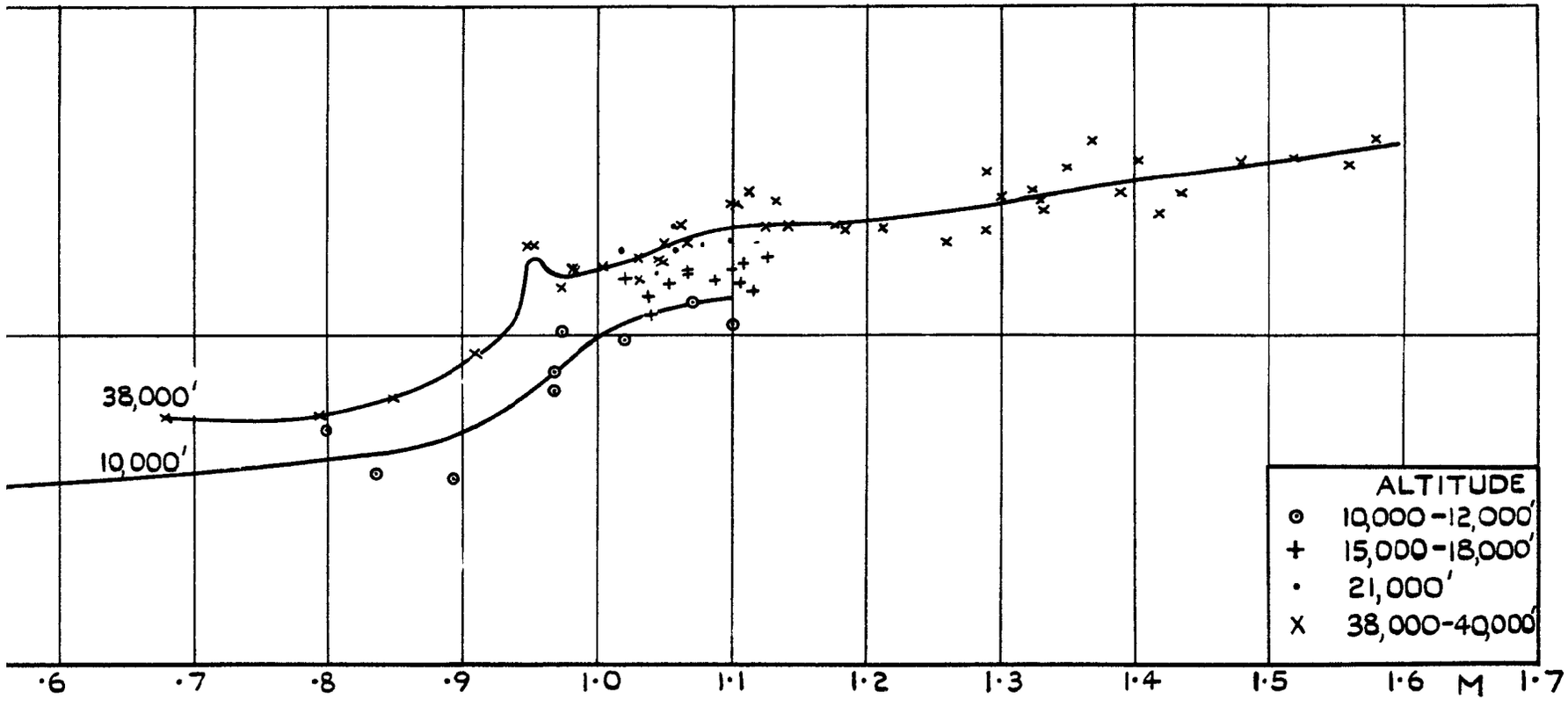

IŒUVRE MARGIN STICK FIXED AS DERIVED FROM FLIGHT TESTS.

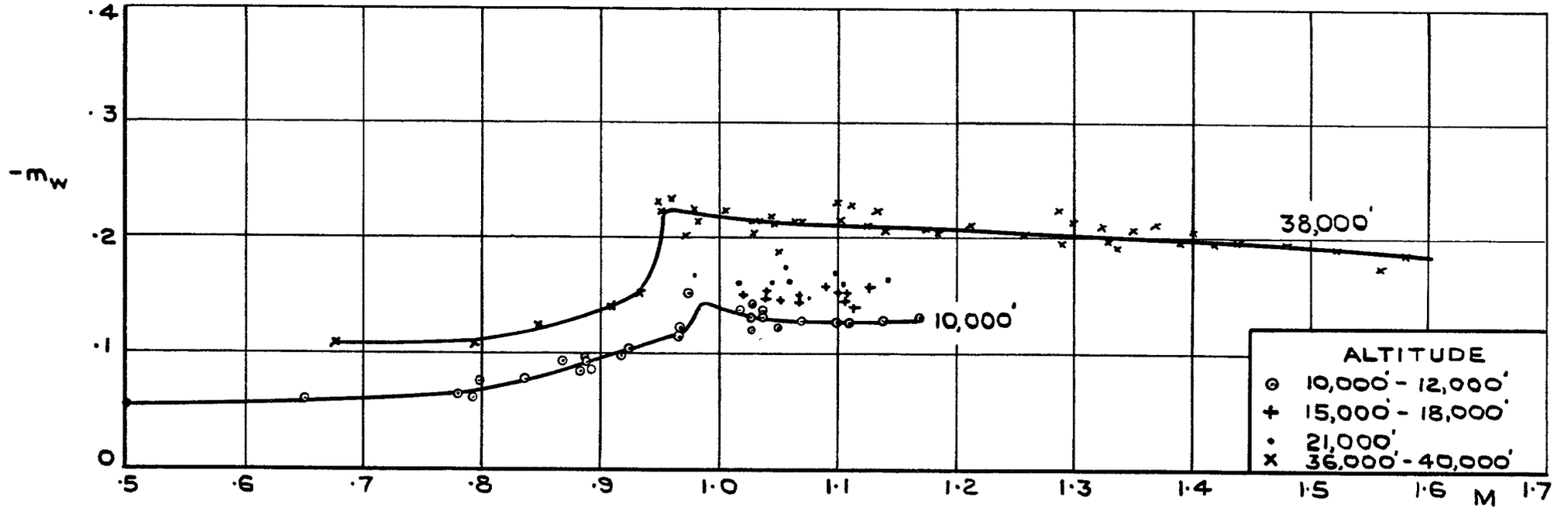

FIG. 14. PITCHING MOMENT DERIVATIVE m_w AS DERIVED FROM FLIGHT TESTS.

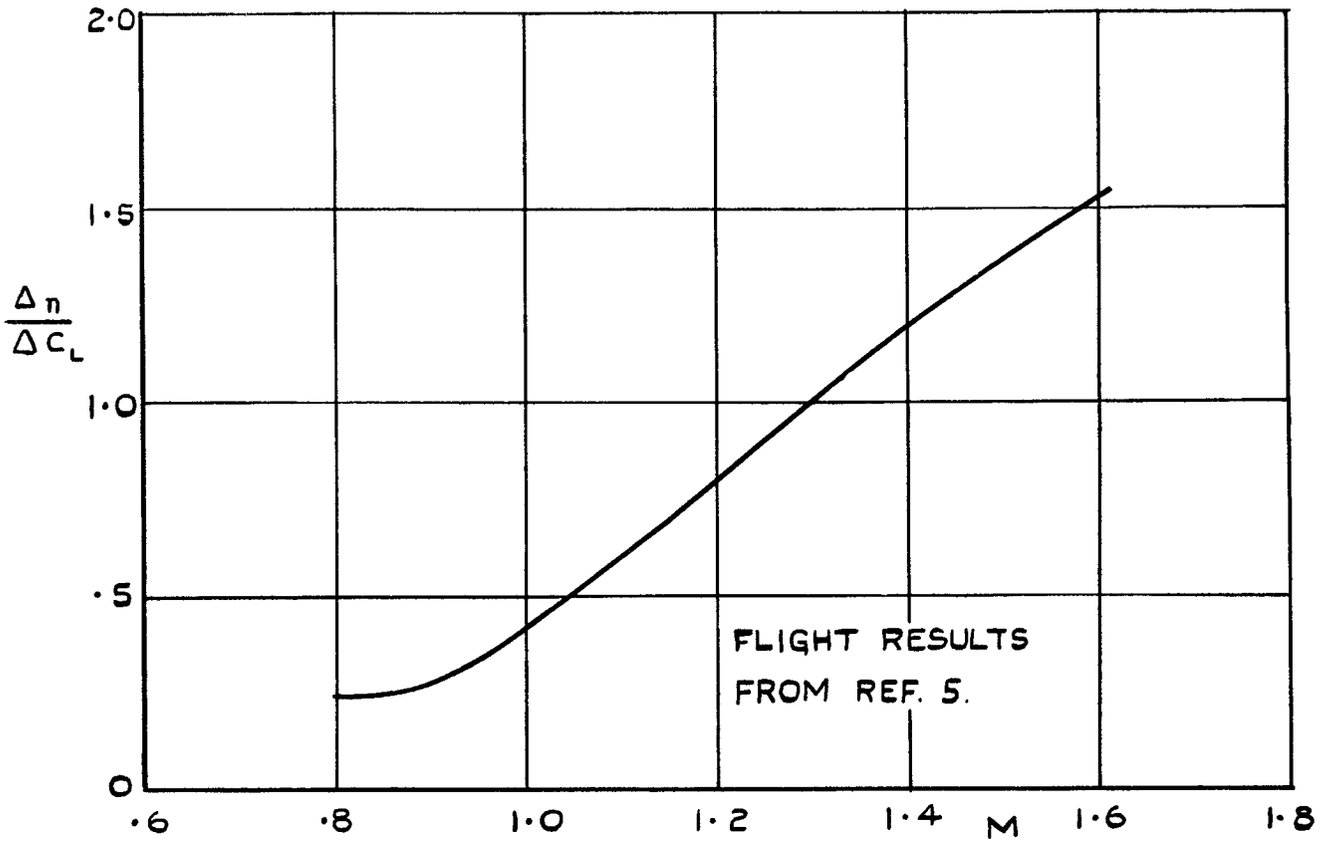

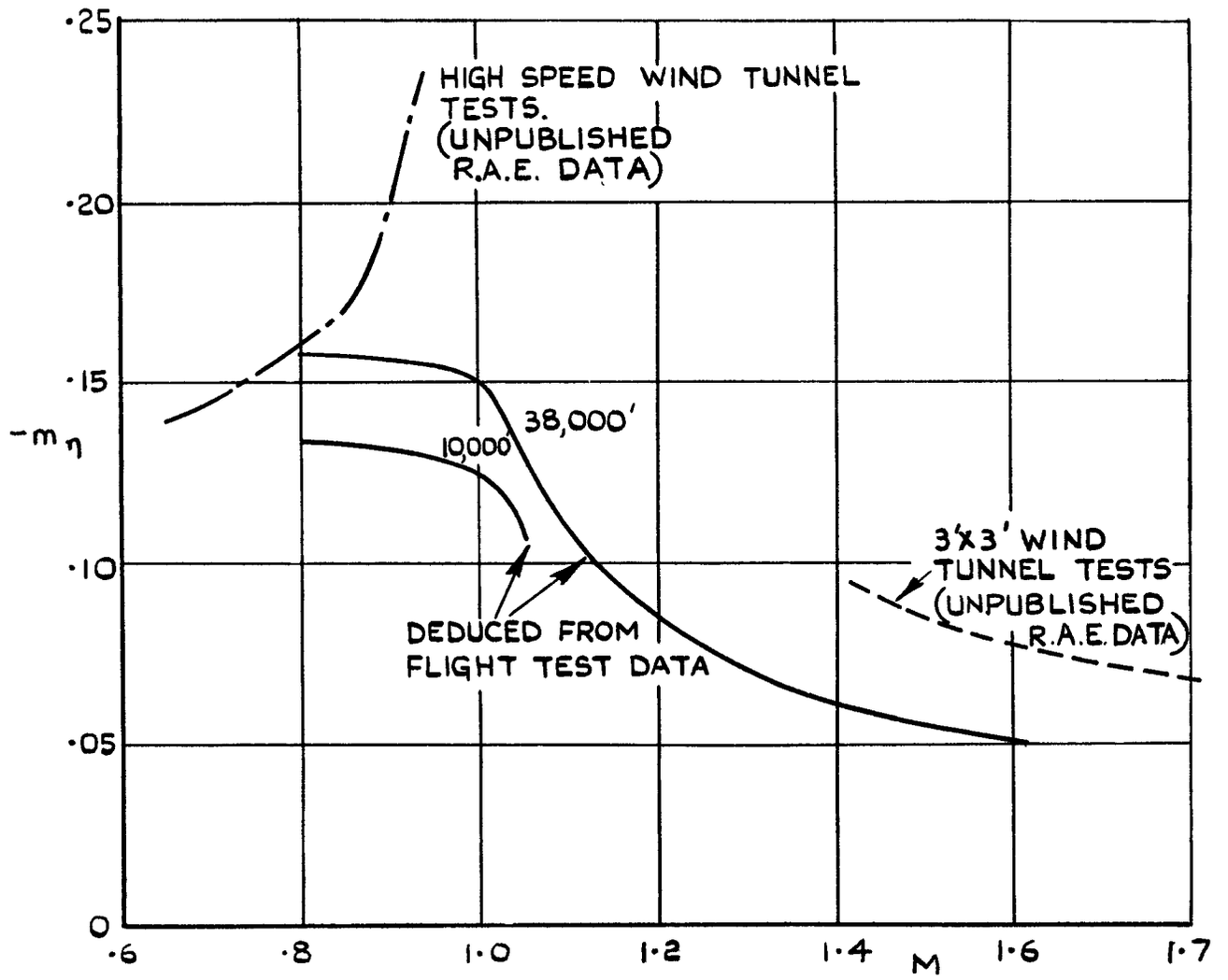

FIG. 15. VALUES OF m_η DERIVED FROM FLIGHT MEASUREMENTS OF H_m AND $\frac{\partial \eta}{\partial C_L}$.

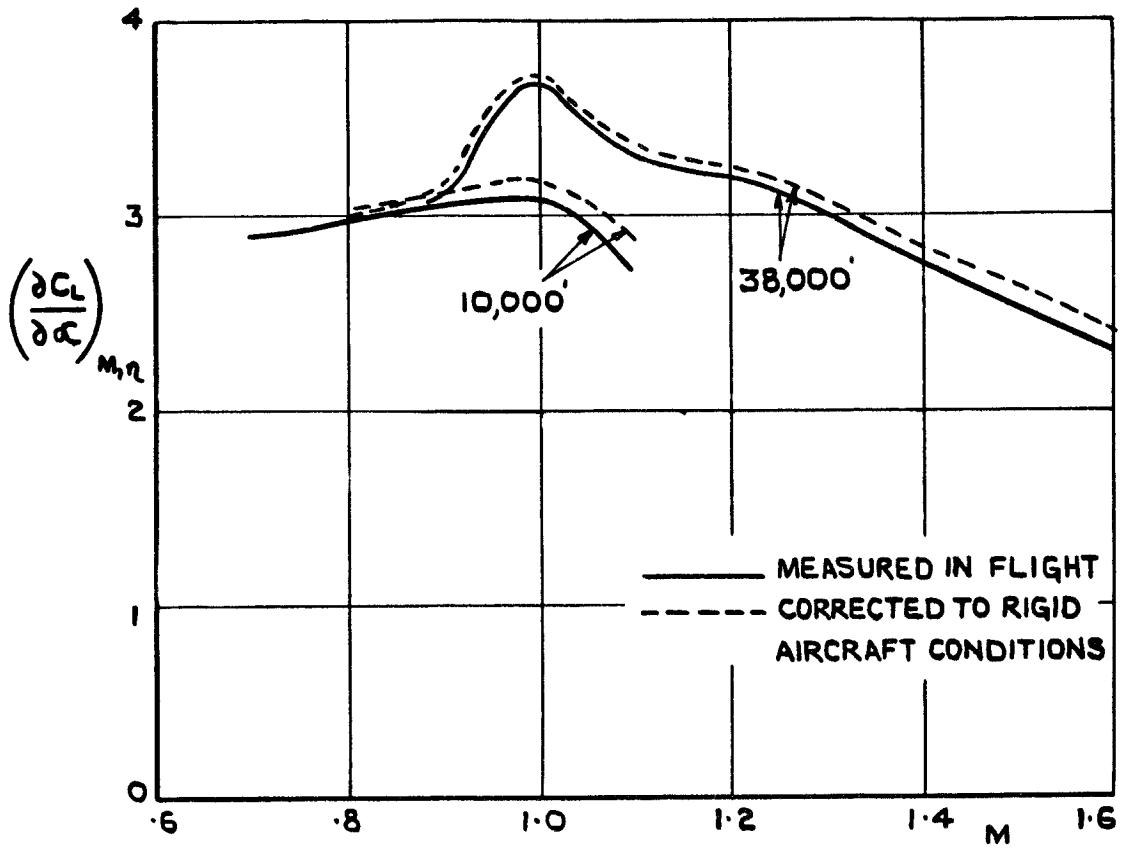

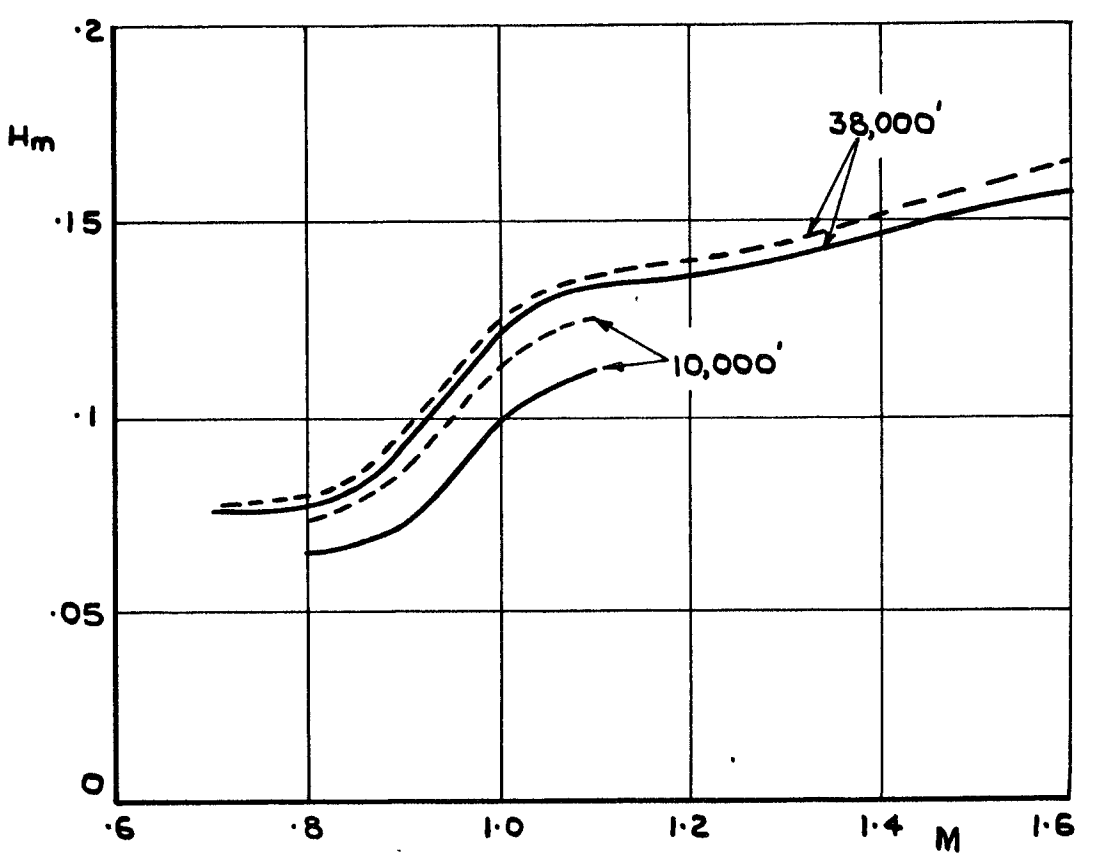

FIG. 16 . EFFECT OF AEROELASTICITY ON THE DERIVATIVES $\frac{\partial C_L}{\partial \alpha}$ AND H_m.

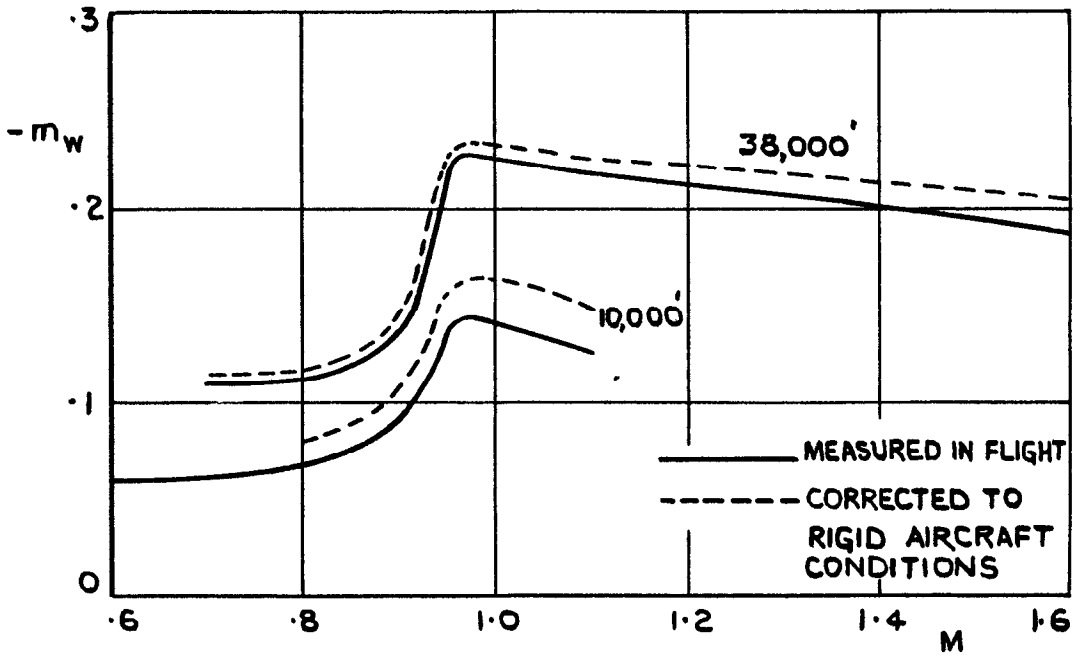
·3
·2
·1
0
$-m_w$
38,000'
10,000'
MEASURED IN FLIGHT
CORRECTED TO RIGID AIRCRAFT CONDITIONS
·6
·8
1·0
1·2
1·4
1·6
M

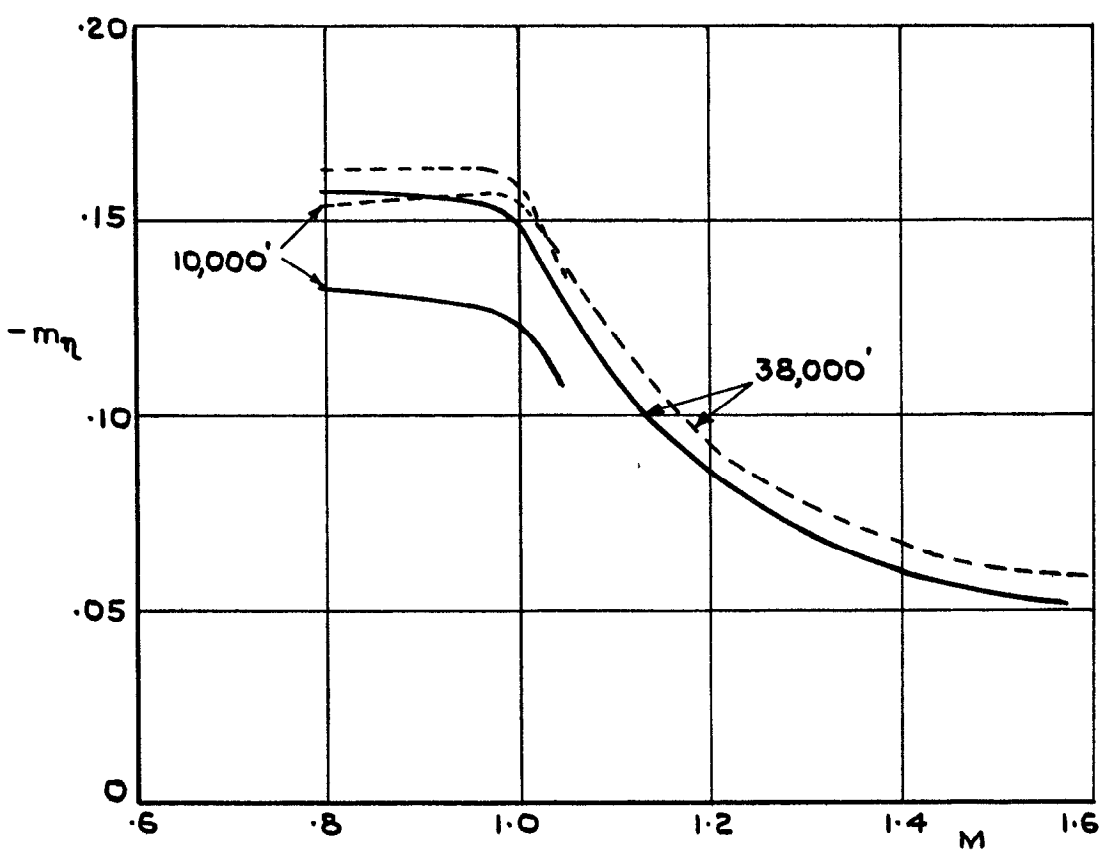
·20
·15
·10
·05
0
$-m_\eta$
10,000'
38,000'
·6
·8
1·0
1·2
1·4
1·6
M

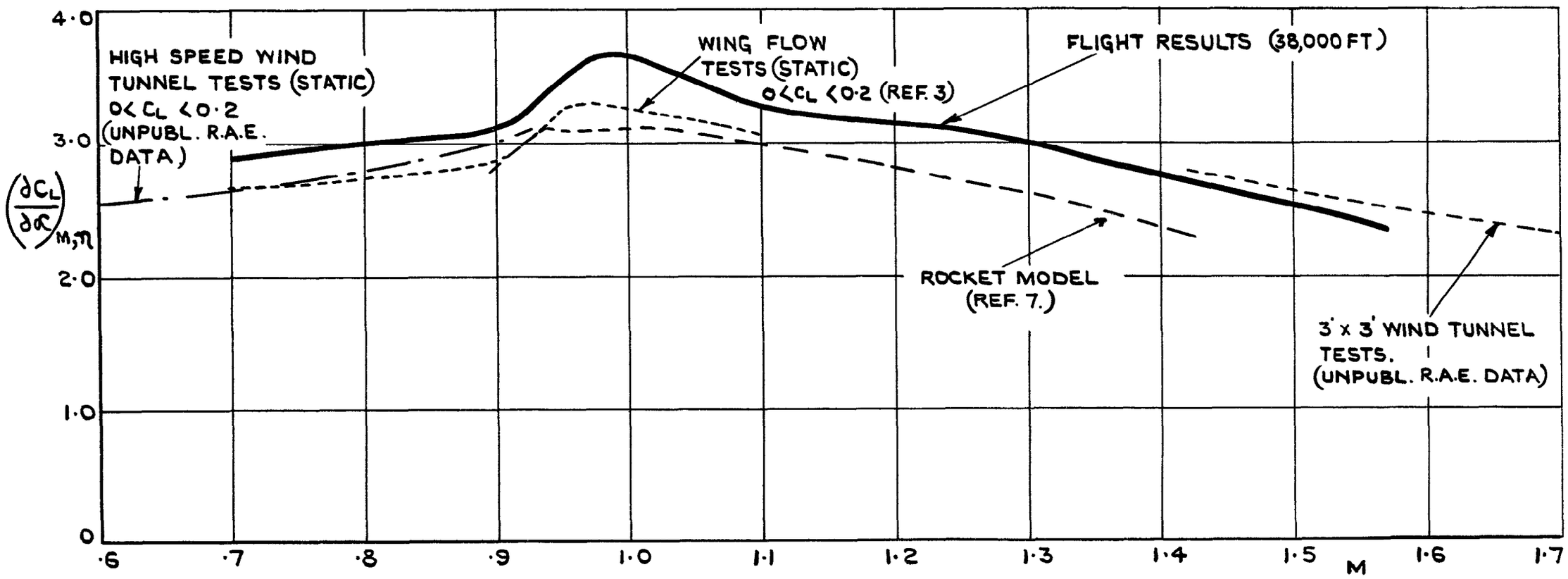

FIG. 18 . COMPARISON OF VALUES OF $\left(\frac{\partial C_L}{\partial \alpha}\right)_{M,\eta}$ FROM FLIGHT AND MODEL TESTS.

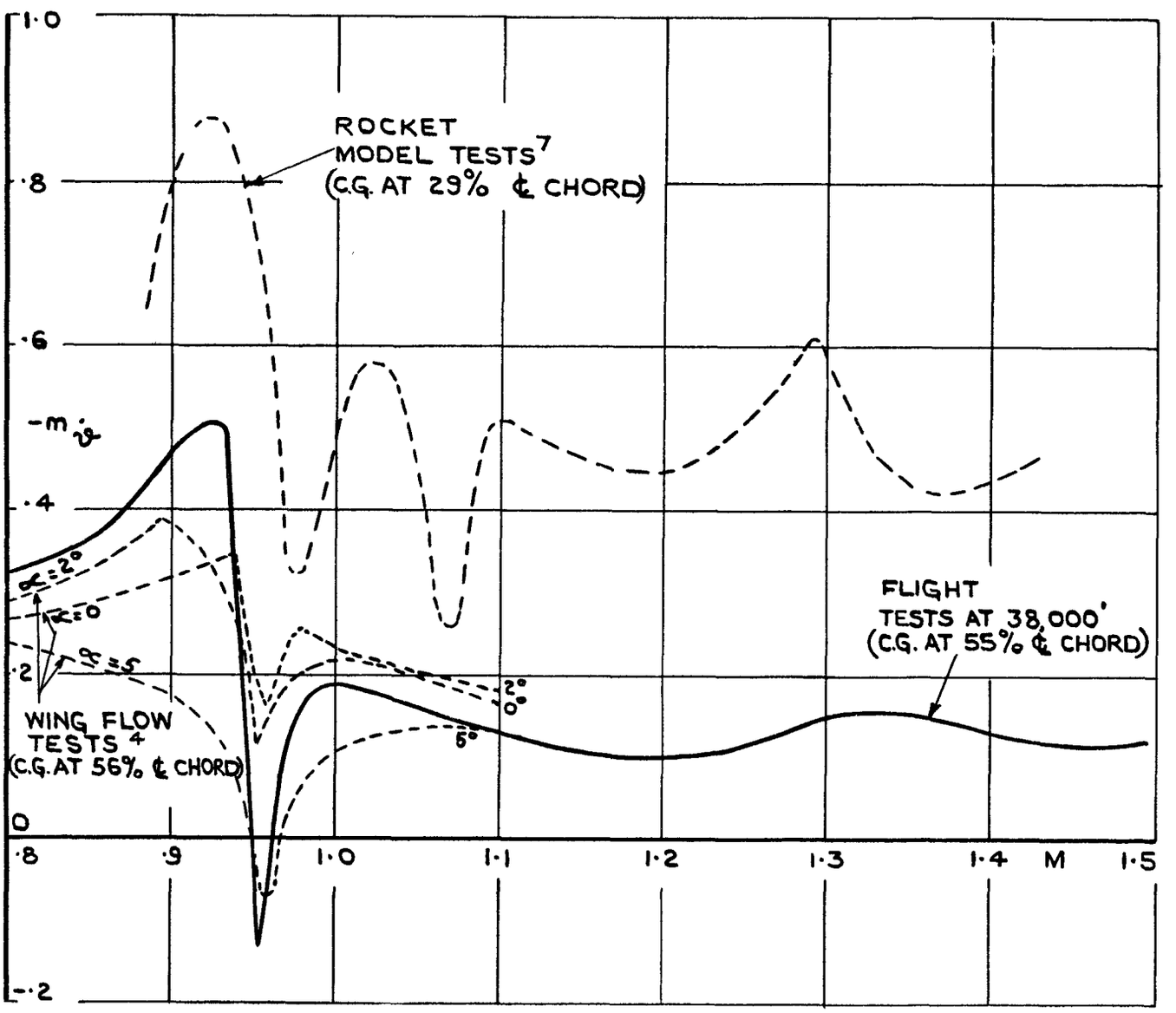

FIG. 19. COMPARISON OF VALUES OF $-m_{\dot{\alpha}}$ FROM FLIGHT AND MODEL TESTS.

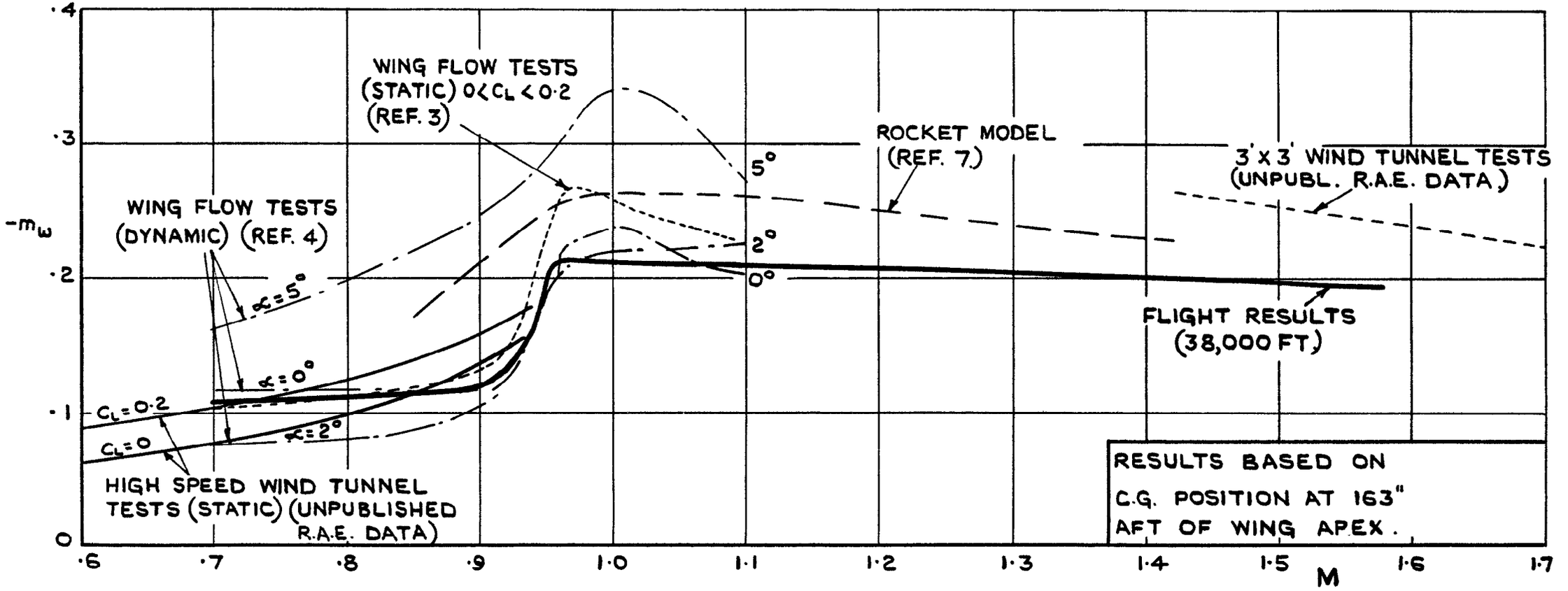

FIG.20 .COMPARISON OF VALUES OF $-m_w$. FROM FLIGHT AND MODEL TESTS.

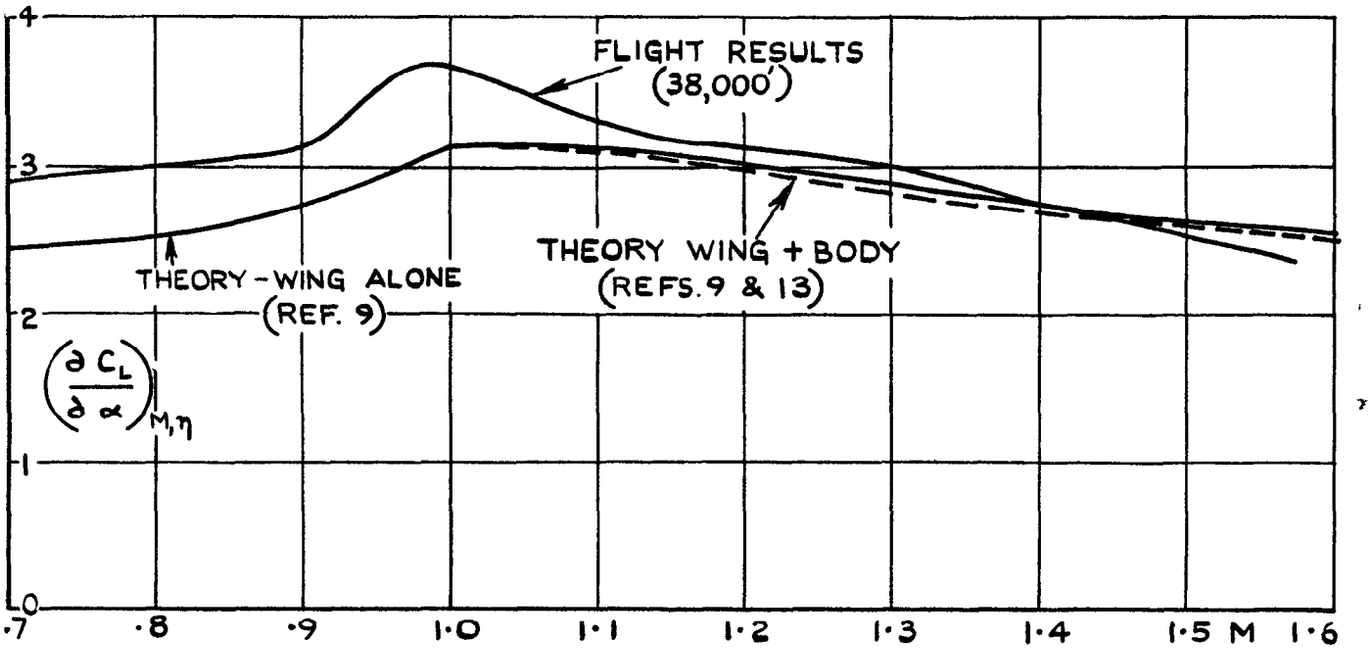
FLIGHT RESULTS
(38,000′)
THEORY WING + BODY
(REFS. 9 & 13)
THEORY - WING ALONE
(REF. 9)
$\left(\frac{\partial C_L}{\partial \alpha}\right)_{M,\eta}$
4
3
2
1
0
·7
·8
·9
1·0
1·1
1·2
1·3
1·4
1·5 M
1·6

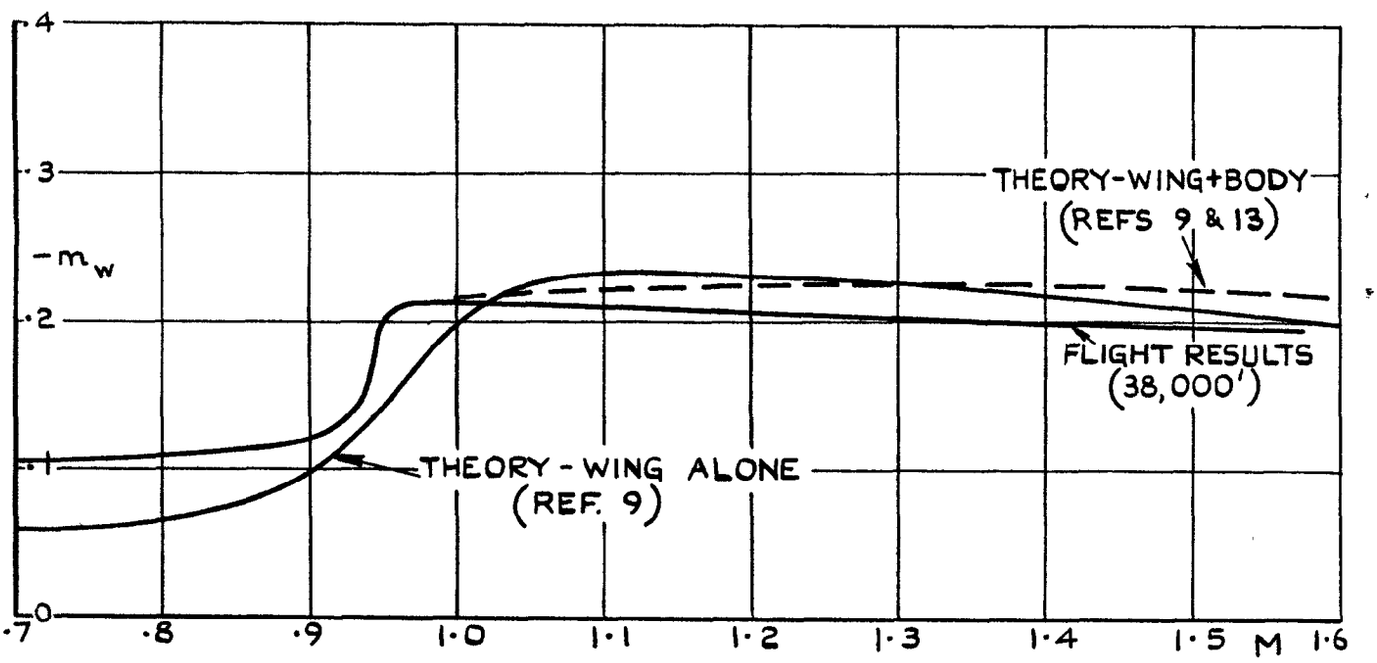
THEORY-WING+BODY
(REFS 9 & 13)
FLIGHT RESULTS
(38,000′)
THEORY - WING ALONE
(REF. 9)
$-m_w$
·4
·3
·2
·1
0
·7
·8
·9
1·0
1·1
1·2
1·3
1·4
1·5
M
1·6

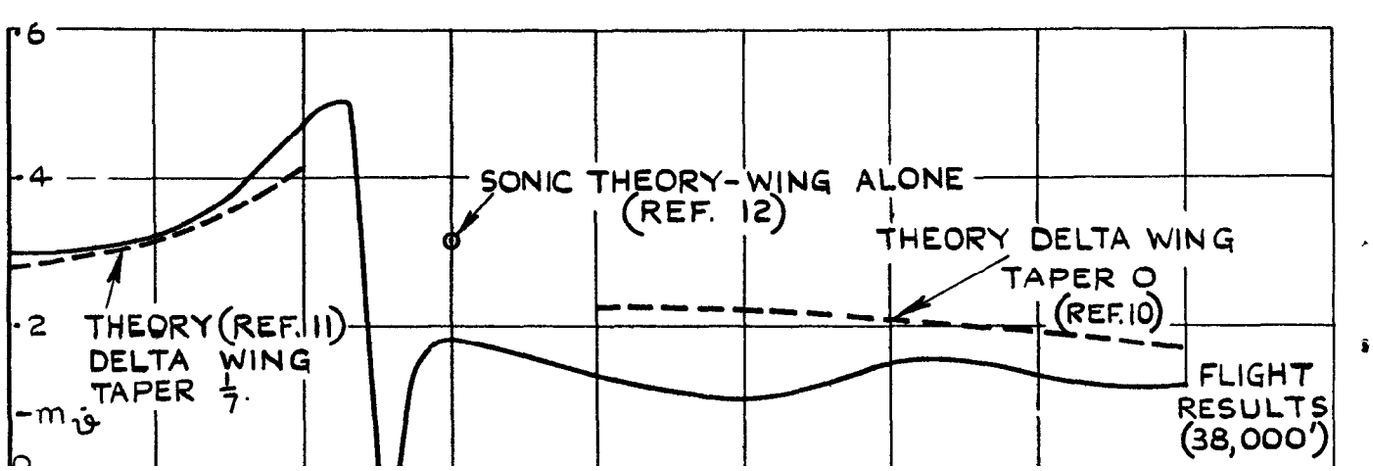
SONIC THEORY-WING ALONE
(REF. 12)
THEORY DELTA WING
TAPER O
(REF.10)
THEORY (REF.11)
DELTA WING
TAPER ⅓
FLIGHT
RESULTS
(38,000′)
$-m_{\dot{w}}$
·6
·4
·2
0

A.R.C. C.P. No.639

533.6.013.412 :
533.6.013.417 :
533.6.053
Fairey Delta 2

MEASUREMENTS IN FLIGHT OF THE LONGITUDINAL STABILITY DERIVATIVES OF A 60° DELTA WING AIRCRAFT (FAIREY DELTA 2)

Andrews, D.R. April 1959.

1.8.1.2.1
1.8.1.2.3
1.7.1.2

Longitudinal short period oscillations have been excited in flight on the Fairey Delta 2 aircraft by stick pulses, and the results analysed to give some of the longitudinal derivatives. Values of the derivatives m_ϑ, $\partial C_L/\partial\alpha$, H_m and m_w are presented for a Mach number range up to M = 1.6 at 38,000 ft altitude and M = 1.15 at 10,000 ft altitude. Some values of m_η have also been derived.

Comparison is made with wind tunnel, rocket model, and wing flow test results, and also with theoretical estimates.

A.R.C. C.P. No.639

533.6.013.412 :
533.6.013.417 :
533.6.053
Fairey Delta 2

MEASUREMENTS IN FLIGHT OF THE LONGITUDINAL STABILITY DERIVATIVES OF A 60° DELTA WING AIRCRAFT (FAIREY DELTA 2)

Andrews, D.R. April 1959.

1.8.1.2.1
1.8.1.2.3
1.7.1.2

Longitudinal short period oscillations have been excited in flight on the Fairey Delta 2 aircraft by stick pulses, and the results analysed to give some of the longitudinal derivatives. Values of the derivatives m_ϑ, $\partial C_L/\partial\alpha$, H_m and m_w are presented for a Mach number range up to M = 1.6 at 38,000 ft altitude and M = 1.15 at 10,000 ft altitude. Some values of m_η have also been derived.

Comparison is made with wind tunnel, rocket model, and wing flow test results, and also with theoretical estimates.

Published by
HER MAJESTY'S STATIONERY OFFICE

To be purchased from
York House, Kingsway, London w.c.2
423 Oxford Street, London w.1
13A Castle Street, Edinburgh 2
109 St. Mary Street, Cardiff
39 King Street, Manchester 2
50 Fairfax Street, Bristol 1
35 Smallbrook, Ringway, Birmingham 5
80 Chichester Street, Belfast 1
or through any bookseller

Printed in England

S.O. CODE No. 23-9013-39